

# Search for Standard Model Higgs Boson Production in Association with a $W$ Boson at CDF

T. Aaltonen,<sup>24</sup> J. Adelman,<sup>14</sup> T. Akimoto,<sup>55</sup> M.G. Albrow,<sup>18</sup> B. Álvarez González,<sup>12</sup>  
 S. Amerio<sup>u</sup>,<sup>43</sup> D. Amidei,<sup>35</sup> A. Anastassov,<sup>38</sup> A. Annovi,<sup>20</sup> J. Antos,<sup>15</sup> G. Apollinari,<sup>18</sup>  
 A. Apresyan,<sup>48</sup> T. Arisawa,<sup>57</sup> A. Artikov,<sup>16</sup> W. Ashmanskas,<sup>18</sup> A. Attal,<sup>4</sup> A. Aurisano,<sup>53</sup>  
 F. Azfar,<sup>42</sup> P. Azzurri<sup>s</sup>,<sup>46</sup> W. Badgett,<sup>18</sup> A. Barbaro-Galtieri,<sup>29</sup> V.E. Barnes,<sup>48</sup>  
 B.A. Barnett,<sup>26</sup> V. Bartsch,<sup>31</sup> G. Bauer,<sup>33</sup> P.-H. Beauchemin,<sup>34</sup> F. Bedeschi,<sup>46</sup> P. Bednar,<sup>15</sup>  
 D. Beecher,<sup>31</sup> S. Behari,<sup>26</sup> G. Bellettini<sup>q</sup>,<sup>46</sup> J. Bellinger,<sup>59</sup> D. Benjamin,<sup>17</sup> A. Beretvas,<sup>18</sup>  
 J. Beringer,<sup>29</sup> A. Bhatti,<sup>50</sup> M. Binkley,<sup>18</sup> D. Bisello<sup>u</sup>,<sup>43</sup> I. Bizjak,<sup>31</sup> R.E. Blair,<sup>2</sup>  
 C. Blocker,<sup>7</sup> B. Blumenfeld,<sup>26</sup> A. Bocci,<sup>17</sup> A. Bodek,<sup>49</sup> V. Boisvert,<sup>49</sup> G. Bolla,<sup>48</sup>  
 D. Bortoletto,<sup>48</sup> J. Boudreau,<sup>47</sup> A. Boveia,<sup>11</sup> B. Brau,<sup>11</sup> A. Bridgeman,<sup>25</sup> L. Brigliadori,<sup>43</sup>  
 C. Bromberg,<sup>36</sup> E. Brubaker,<sup>14</sup> J. Budagov,<sup>16</sup> H.S. Budd,<sup>49</sup> S. Budd,<sup>25</sup> K. Burkett,<sup>18</sup>  
 G. Busetto<sup>u</sup>,<sup>43</sup> P. Bussey,<sup>22</sup> A. Buzatu,<sup>34</sup> K. L. Byrum,<sup>2</sup> S. Cabrera<sup>p</sup>,<sup>17</sup> C. Calancha,<sup>32</sup>  
 M. Campanelli,<sup>36</sup> M. Campbell,<sup>35</sup> F. Canelli,<sup>18</sup> A. Canepa,<sup>45</sup> D. Carlsmith,<sup>59</sup> R. Carosi,<sup>46</sup>  
 S. Carrillo<sup>j</sup>,<sup>19</sup> S. Carron,<sup>34</sup> B. Casal,<sup>12</sup> M. Casarsa,<sup>18</sup> A. Castro<sup>t</sup>,<sup>6</sup> P. Catastini<sup>r</sup>,<sup>46</sup>  
 D. Cauz<sup>w</sup>,<sup>54</sup> V. Cavaliere<sup>r</sup>,<sup>46</sup> M. Cavalli-Sforza,<sup>4</sup> A. Cerri,<sup>29</sup> L. Cerrito<sup>n</sup>,<sup>31</sup> S.H. Chang,<sup>28</sup>  
 Y.C. Chen,<sup>1</sup> M. Chertok,<sup>8</sup> G. Chiarelli,<sup>46</sup> G. Chlachidze,<sup>18</sup> F. Chlebana,<sup>18</sup> K. Cho,<sup>28</sup>  
 D. Chokheli,<sup>16</sup> J.P. Chou,<sup>23</sup> G. Choudalakis,<sup>33</sup> S.H. Chuang,<sup>52</sup> K. Chung,<sup>13</sup> W.H. Chung,<sup>59</sup>  
 Y.S. Chung,<sup>49</sup> C.I. Ciobanu,<sup>44</sup> M.A. Ciocci<sup>r</sup>,<sup>46</sup> A. Clark,<sup>21</sup> D. Clark,<sup>7</sup> G. Compostella,<sup>43</sup>  
 M.E. Convery,<sup>18</sup> J. Conway,<sup>8</sup> K. Copic,<sup>35</sup> M. Cordelli,<sup>20</sup> G. Cortiana<sup>u</sup>,<sup>43</sup> D.J. Cox,<sup>8</sup>  
 F. Crescioli<sup>q</sup>,<sup>46</sup> C. Cuenca Almenar<sup>p</sup>,<sup>8</sup> J. Cuevas<sup>m</sup>,<sup>12</sup> R. Culbertson,<sup>18</sup> J.C. Cully,<sup>35</sup>  
 M. Datta,<sup>18</sup> T. Davies,<sup>22</sup> P. de Barbaro,<sup>49</sup> S. De Cecco,<sup>51</sup> A. Deisher,<sup>29</sup> G. De Lorenzo,<sup>4</sup>  
 M. Dell'Orso<sup>q</sup>,<sup>46</sup> C. Deluca,<sup>4</sup> L. Demortier,<sup>50</sup> J. Deng,<sup>17</sup> M. Deninno<sup>t</sup>,<sup>6</sup> P.F. Derwent,<sup>18</sup>  
 G.P. di Giovanni,<sup>44</sup> C. Dionisi<sup>v</sup>,<sup>51</sup> B. Di Ruzza<sup>w</sup>,<sup>54</sup> J.R. Dittmann,<sup>5</sup> M. D'Onofrio,<sup>4</sup>  
 S. Donati<sup>q</sup>,<sup>46</sup> P. Dong,<sup>9</sup> J. Donini,<sup>43</sup> T. Dorigo,<sup>43</sup> S. Dube,<sup>52</sup> J. Efron,<sup>39</sup> A. Elagin,<sup>53</sup>  
 R. Erbacher,<sup>8</sup> D. Errede,<sup>25</sup> S. Errede,<sup>25</sup> R. Eusebi,<sup>18</sup> H.C. Fang,<sup>29</sup> S. Farrington,<sup>42</sup>  
 W.T. Fedorko,<sup>14</sup> R.G. Feild,<sup>60</sup> M. Feindt,<sup>27</sup> J.P. Fernandez,<sup>32</sup> C. Ferrazza<sup>s</sup>,<sup>46</sup> R. Field,<sup>19</sup>  
 G. Flanagan,<sup>48</sup> R. Forrest,<sup>8</sup> M. Franklin,<sup>23</sup> J.C. Freeman,<sup>18</sup> I. Furic,<sup>19</sup> M. Gallinaro,<sup>51</sup>  
 J. Galyardt,<sup>13</sup> F. Garbersen,<sup>11</sup> J.E. Garcia,<sup>46</sup> A.F. Garfinkel,<sup>48</sup> K. Genser,<sup>18</sup> H. Gerberich,<sup>25</sup>  
 D. Gerdes,<sup>35</sup> A. Gessler,<sup>27</sup> S. Giagu<sup>v</sup>,<sup>51</sup> V. Giakoumopoulou,<sup>3</sup> P. Giannetti,<sup>46</sup> K. Gibson,<sup>47</sup>

31 J.L. Gimmell,<sup>49</sup> C.M. Ginsburg,<sup>18</sup> N. Giokaris,<sup>3</sup> M. Giordani<sup>w</sup>,<sup>54</sup> P. Giromini,<sup>20</sup>  
32 M. Giunta<sup>q</sup>,<sup>46</sup> G. Giurgiu,<sup>26</sup> V. Glagolev,<sup>16</sup> D. Glenzinski,<sup>18</sup> M. Gold,<sup>37</sup> N. Goldschmidt,<sup>19</sup>  
33 A. Golossanov,<sup>18</sup> G. Gomez,<sup>12</sup> G. Gomez-Ceballos,<sup>33</sup> M. Goncharov,<sup>53</sup> O. González,<sup>32</sup>  
34 I. Gorelov,<sup>37</sup> A.T. Goshaw,<sup>17</sup> K. Goulianos,<sup>50</sup> A. Gresele<sup>u</sup>,<sup>43</sup> S. Grinstein,<sup>23</sup>  
35 C. Grosso-Pilcher,<sup>14</sup> R.C. Group,<sup>18</sup> U. Grundler,<sup>25</sup> J. Guimaraes da Costa,<sup>23</sup>  
36 Z. Gunay-Unalan,<sup>36</sup> C. Haber,<sup>29</sup> K. Hahn,<sup>33</sup> S.R. Hahn,<sup>18</sup> E. Halkiadakis,<sup>52</sup> B.-Y. Han,<sup>49</sup>  
37 J.Y. Han,<sup>49</sup> R. Handler,<sup>59</sup> F. Happacher,<sup>20</sup> K. Hara,<sup>55</sup> D. Hare,<sup>52</sup> M. Hare,<sup>56</sup> S. Harper,<sup>42</sup>  
38 R.F. Harr,<sup>58</sup> R.M. Harris,<sup>18</sup> M. Hartz,<sup>47</sup> K. Hatakeyama,<sup>50</sup> J. Hauser,<sup>9</sup> C. Hays,<sup>42</sup>  
39 M. Heck,<sup>27</sup> A. Heijboer,<sup>45</sup> B. Heinemann,<sup>29</sup> J. Heinrich,<sup>45</sup> C. Henderson,<sup>33</sup> M. Herndon,<sup>59</sup>  
40 J. Heuser,<sup>27</sup> S. Hewamanage,<sup>5</sup> D. Hidas,<sup>17</sup> C.S. Hill<sup>c</sup>,<sup>11</sup> D. Hirschbuehl,<sup>27</sup> A. Hocker,<sup>18</sup>  
41 S. Hou,<sup>1</sup> M. Houlden,<sup>30</sup> S.-C. Hsu,<sup>10</sup> B.T. Huffman,<sup>42</sup> R.E. Hughes,<sup>39</sup> U. Husemann,<sup>60</sup>  
42 J. Huston,<sup>36</sup> J. Incandela,<sup>11</sup> G. Introzzi,<sup>46</sup> M. Iori<sup>v</sup>,<sup>51</sup> A. Ivanov,<sup>8</sup> E. James,<sup>18</sup>  
43 B. Jayatilaka,<sup>17</sup> E.J. Jeon,<sup>28</sup> S. Jindariani,<sup>18</sup> W. Johnson,<sup>8</sup> M. Jones,<sup>48</sup> K.K. Joo,<sup>28</sup>  
44 S.Y. Jun,<sup>13</sup> J.E. Jung,<sup>28</sup> T.R. Junk,<sup>18</sup> T. Kamon,<sup>53</sup> D. Kar,<sup>19</sup> P.E. Karchin,<sup>58</sup> Y. Kato,<sup>41</sup>  
45 R. Kephart,<sup>18</sup> J. Keung,<sup>45</sup> V. Khotilovich,<sup>53</sup> B. Kilminster,<sup>39</sup> D.H. Kim,<sup>28</sup> H.S. Kim,<sup>28</sup>  
46 J.E. Kim,<sup>28</sup> M.J. Kim,<sup>20</sup> S.B. Kim,<sup>28</sup> S.H. Kim,<sup>55</sup> Y.K. Kim,<sup>14</sup> N. Kimura,<sup>55</sup> L. Kirsch,<sup>7</sup>  
47 S. Klimenko,<sup>19</sup> B. Knuteson,<sup>33</sup> B.R. Ko,<sup>17</sup> S.A. Koay,<sup>11</sup> K. Kondo,<sup>57</sup> D.J. Kong,<sup>28</sup>  
48 J. Konigsberg,<sup>19</sup> A. Korytov,<sup>19</sup> A.V. Kotwal,<sup>17</sup> M. Kreps,<sup>27</sup> J. Kroll,<sup>45</sup> N. Krumnack,<sup>5</sup>  
49 M. Kruse,<sup>17</sup> V. Krutelyov,<sup>11</sup> T. Kubo,<sup>55</sup> T. Kuhr,<sup>27</sup> N.P. Kulkarni,<sup>58</sup> M. Kurata,<sup>55</sup>  
50 Y. Kusakabe,<sup>57</sup> S. Kwang,<sup>14</sup> A.T. Laasanen,<sup>48</sup> S. Lami,<sup>46</sup> S. Lammel,<sup>18</sup> M. Lancaster,<sup>31</sup>  
51 R.L. Lander,<sup>8</sup> K. Lannon,<sup>39</sup> A. Lath,<sup>52</sup> G. Latino<sup>r</sup>,<sup>46</sup> I. Lazzizzera<sup>u</sup>,<sup>43</sup> T. LeCompte,<sup>2</sup>  
52 E. Lee,<sup>53</sup> J. Lee,<sup>28</sup> Y.J. Lee,<sup>28</sup> S.W. Lee<sup>o</sup>,<sup>53</sup> S. Leone,<sup>46</sup> S. Levy,<sup>14</sup> J.D. Lewis,<sup>18</sup> C.S. Lin,<sup>29</sup>  
53 J. Linacre,<sup>42</sup> M. Lindgren,<sup>18</sup> E. Lipeles,<sup>10</sup> A. Lister,<sup>8</sup> D.O. Litvintsev,<sup>18</sup> C. Liu,<sup>47</sup> T. Liu,<sup>18</sup>  
54 N.S. Lockyer,<sup>45</sup> A. Loginov,<sup>60</sup> M. Loreti<sup>u</sup>,<sup>43</sup> L. Lovas,<sup>15</sup> R.-S. Lu,<sup>1</sup> D. Lucchesi<sup>u</sup>,<sup>43</sup>  
55 J. Lueck,<sup>27</sup> C. Luci<sup>v</sup>,<sup>51</sup> P. Lujan,<sup>29</sup> P. Lukens,<sup>18</sup> G. Lungu,<sup>50</sup> L. Lyons,<sup>42</sup> J. Lys,<sup>29</sup>  
56 R. Lysak,<sup>15</sup> E. Lytken,<sup>48</sup> P. Mack,<sup>27</sup> D. MacQueen,<sup>34</sup> R. Madrak,<sup>18</sup> K. Maeshima,<sup>18</sup>  
57 K. Makhoul,<sup>33</sup> T. Maki,<sup>24</sup> P. Maksimovic,<sup>26</sup> S. Malde,<sup>42</sup> S. Malik,<sup>31</sup> G. Manca,<sup>30</sup>  
58 A. Manousakis-Katsikakis,<sup>3</sup> F. Margaroli,<sup>48</sup> C. Marino,<sup>27</sup> C.P. Marino,<sup>25</sup> A. Martin,<sup>60</sup>  
59 V. Martin<sup>i</sup>,<sup>22</sup> M. Martínez,<sup>4</sup> R. Martínez-Ballarín,<sup>32</sup> T. Maruyama,<sup>55</sup> P. Mastrandrea<sup>v</sup>,<sup>51</sup>  
60 T. Masubuchi,<sup>55</sup> M.E. Mattson,<sup>58</sup> P. Mazzanti,<sup>6</sup> K.S. McFarland,<sup>49</sup> P. McIntyre,<sup>53</sup>

61 R. McNulty<sup>h</sup>,<sup>30</sup> A. Mehta,<sup>30</sup> P. Mehtala,<sup>24</sup> A. Menzione,<sup>46</sup> P. Merkel,<sup>48</sup> C. Mesropian,<sup>50</sup>  
 62 T. Miao,<sup>18</sup> N. Miladinovic,<sup>7</sup> R. Miller,<sup>36</sup> C. Mills,<sup>23</sup> M. Milnik,<sup>27</sup> A. Mitra,<sup>1</sup>  
 63 G. Mitselmakher,<sup>19</sup> H. Miyake,<sup>55</sup> N. Moggi,<sup>6</sup> C.S. Moon,<sup>28</sup> R. Moore,<sup>18</sup> M.J. Morello<sup>q</sup>,<sup>46</sup>  
 64 J. Morlok,<sup>27</sup> P. Movilla Fernandez,<sup>18</sup> J. Mülmenstädt,<sup>29</sup> A. Mukherjee,<sup>18</sup> Th. Muller,<sup>27</sup>  
 65 R. Mumford,<sup>26</sup> P. Murat,<sup>18</sup> M. Mussini<sup>t</sup>,<sup>6</sup> J. Nachtman,<sup>18</sup> Y. Nagai,<sup>55</sup> A. Nagano,<sup>55</sup>  
 66 J. Naganoma,<sup>57</sup> K. Nakamura,<sup>55</sup> I. Nakano,<sup>40</sup> A. Napier,<sup>56</sup> V. Necula,<sup>17</sup> C. Neu,<sup>45</sup>  
 67 M.S. Neubauer,<sup>25</sup> J. Nielsen<sup>e</sup>,<sup>29</sup> L. Nodulman,<sup>2</sup> M. Norman,<sup>10</sup> O. Norniella,<sup>25</sup> E. Nurse,<sup>31</sup>  
 68 L. Oakes,<sup>42</sup> S.H. Oh,<sup>17</sup> Y.D. Oh,<sup>28</sup> I. Oksuzian,<sup>19</sup> T. Okusawa,<sup>41</sup> R. Orava,<sup>24</sup> K. Osterberg,<sup>24</sup>  
 69 S. Pagan Griso<sup>u</sup>,<sup>43</sup> C. Pagliarone,<sup>46</sup> E. Palencia,<sup>18</sup> V. Papadimitriou,<sup>18</sup> A. Papaikonomou,<sup>27</sup>  
 70 A.A. Paramonov,<sup>14</sup> B. Parks,<sup>39</sup> S. Pashapour,<sup>34</sup> J. Patrick,<sup>18</sup> G. Pauletta<sup>w</sup>,<sup>54</sup> M. Paulini,<sup>13</sup>  
 71 C. Paus,<sup>33</sup> D.E. Pellett,<sup>8</sup> A. Penzo,<sup>54</sup> T.J. Phillips,<sup>17</sup> G. Piacentino,<sup>46</sup> E. Pianori,<sup>45</sup>  
 72 L. Pinera,<sup>19</sup> K. Pitts,<sup>25</sup> C. Plager,<sup>9</sup> L. Pondrom,<sup>59</sup> O. Poukhov,<sup>16</sup> N. Pounder,<sup>42</sup>  
 73 F. Prakoshyn,<sup>16</sup> A. Pronko,<sup>18</sup> J. Proudfoot,<sup>2</sup> F. Ptohos<sup>g</sup>,<sup>18</sup> E. Pueschel,<sup>13</sup> G. Punzi<sup>a</sup>,<sup>46</sup>  
 74 J. Pursley,<sup>59</sup> J. Rademacker<sup>c</sup>,<sup>42</sup> A. Rahaman,<sup>47</sup> V. Ramakrishnan,<sup>59</sup> N. Ranjan,<sup>48</sup>  
 75 I. Redondo,<sup>32</sup> B. Reisert,<sup>18</sup> V. Rekovic,<sup>37</sup> P. Renton,<sup>42</sup> M. Rescigno,<sup>51</sup> S. Richter,<sup>27</sup>  
 76 F. Rimondi<sup>t</sup>,<sup>6</sup> L. Ristori,<sup>46</sup> A. Robson,<sup>22</sup> T. Rodrigo,<sup>12</sup> T. Rodriguez,<sup>45</sup> E. Rogers,<sup>25</sup>  
 77 S. Rolli,<sup>56</sup> R. Roser,<sup>18</sup> M. Rossi,<sup>54</sup> R. Rossin,<sup>11</sup> P. Roy,<sup>34</sup> A. Ruiz,<sup>12</sup> J. Russ,<sup>13</sup>  
 78 V. Rusu,<sup>18</sup> H. Saarikko,<sup>24</sup> A. Safonov,<sup>53</sup> W.K. Sakumoto,<sup>49</sup> O. Saltó,<sup>4</sup> L. Santi<sup>w</sup>,<sup>54</sup>  
 79 S. Sarkar<sup>v</sup>,<sup>51</sup> L. Sartori,<sup>46</sup> K. Sato,<sup>18</sup> A. Savoy-Navarro,<sup>44</sup> T. Scheidle,<sup>27</sup> P. Schlabach,<sup>18</sup>  
 80 A. Schmidt,<sup>27</sup> E.E. Schmidt,<sup>18</sup> M.A. Schmidt,<sup>14</sup> M.P. Schmidt,<sup>60</sup> M. Schmitt,<sup>38</sup>  
 81 T. Schwarz,<sup>8</sup> L. Scodellaro,<sup>12</sup> A.L. Scott,<sup>11</sup> A. Scribano<sup>r</sup>,<sup>46</sup> F. Scuri,<sup>46</sup> A. Sedov,<sup>48</sup>  
 82 S. Seidel,<sup>37</sup> Y. Seiya,<sup>41</sup> A. Semenov,<sup>16</sup> L. Sexton-Kennedy,<sup>18</sup> A. Sfyrla,<sup>21</sup> S.Z. Shalhout,<sup>58</sup>  
 83 T. Shears,<sup>30</sup> P.F. Shepard,<sup>47</sup> D. Sherman,<sup>23</sup> M. Shimojima<sup>l</sup>,<sup>55</sup> M. Shochet,<sup>14</sup> Y. Shon,<sup>59</sup>  
 84 I. Shreyber,<sup>21</sup> A. Sidoti,<sup>46</sup> P. Sinervo,<sup>34</sup> A. Sisakyan,<sup>16</sup> A.J. Slaughter,<sup>18</sup> J. Slaunwhite,<sup>39</sup>  
 85 K. Sliwa,<sup>56</sup> J.R. Smith,<sup>8</sup> F.D. Snider,<sup>18</sup> R. Snihur,<sup>34</sup> A. Soha,<sup>8</sup> S. Somalwar,<sup>52</sup> V. Sorin,<sup>36</sup>  
 86 J. Spalding,<sup>18</sup> T. Spreitzer,<sup>34</sup> P. Squillacioti<sup>r</sup>,<sup>46</sup> M. Stanitzki,<sup>60</sup> R. St. Denis,<sup>22</sup>  
 87 B. Stelzer,<sup>9</sup> O. Stelzer-Chilton,<sup>42</sup> D. Stentz,<sup>38</sup> J. Strologas,<sup>37</sup> D. Stuart,<sup>11</sup> J.S. Suh,<sup>28</sup>  
 88 A. Sukhanov,<sup>19</sup> I. Suslov,<sup>16</sup> T. Suzuki,<sup>55</sup> A. Taffard<sup>d</sup>,<sup>25</sup> R. Takashima,<sup>40</sup> Y. Takeuchi,<sup>55</sup>  
 89 R. Tanaka,<sup>40</sup> M. Tecchio,<sup>35</sup> P.K. Teng,<sup>1</sup> K. Terashi,<sup>50</sup> J. Thom<sup>f</sup>,<sup>18</sup> A.S. Thompson,<sup>22</sup>  
 90 G.A. Thompson,<sup>25</sup> E. Thomson,<sup>45</sup> P. Tipton,<sup>60</sup> V. Tiwari,<sup>13</sup> S. Tkaczyk,<sup>18</sup> D. Toback,<sup>53</sup>

91 S. Tokar,<sup>15</sup> K. Tollefson,<sup>36</sup> T. Tomura,<sup>55</sup> D. Tonelli,<sup>18</sup> S. Torre,<sup>20</sup> D. Torretta,<sup>18</sup>  
 92 P. Totaro<sup>w</sup>,<sup>54</sup> S. Tourneur,<sup>44</sup> Y. Tu,<sup>45</sup> N. Turini<sup>r</sup>,<sup>46</sup> F. Ukegawa,<sup>55</sup> S. Vallecorsa,<sup>21</sup>  
 93 N. van Remortel<sup>a</sup>,<sup>24</sup> A. Varganov,<sup>35</sup> E. Vataga<sup>s</sup>,<sup>46</sup> F. Vázquez<sup>j</sup>,<sup>19</sup> G. Velez,<sup>18</sup> C. Vellidis,<sup>3</sup>  
 94 V. Veszpremi,<sup>48</sup> M. Vidal,<sup>32</sup> R. Vidal,<sup>18</sup> I. Vila,<sup>12</sup> R. Vilar,<sup>12</sup> T. Vine,<sup>31</sup> M. Vogel,<sup>37</sup>  
 95 I. Volobouev<sup>o</sup>,<sup>29</sup> G. Volpi<sup>q</sup>,<sup>46</sup> F. Würthwein,<sup>10</sup> P. Wagner,<sup>2</sup> R.G. Wagner,<sup>2</sup> R.L. Wagner,<sup>18</sup>  
 96 J. Wagner-Kuhr,<sup>27</sup> W. Wagner,<sup>27</sup> T. Wakisaka,<sup>41</sup> R. Wallny,<sup>9</sup> S.M. Wang,<sup>1</sup> A. Warburton,<sup>34</sup>  
 97 D. Waters,<sup>31</sup> M. Weinberger,<sup>53</sup> W.C. Wester III,<sup>18</sup> B. Whitehouse,<sup>56</sup> D. Whiteson<sup>d</sup>,<sup>45</sup>  
 98 A.B. Wicklund,<sup>2</sup> E. Wicklund,<sup>18</sup> G. Williams,<sup>34</sup> H.H. Williams,<sup>45</sup> P. Wilson,<sup>18</sup> B.L. Winer,<sup>39</sup>  
 99 P. Wittich<sup>f</sup>,<sup>18</sup> S. Wolbers,<sup>18</sup> C. Wolfe,<sup>14</sup> T. Wright,<sup>35</sup> X. Wu,<sup>21</sup> S.M. Wynne,<sup>30</sup> A. Yagil,<sup>10</sup>  
 100 K. Yamamoto,<sup>41</sup> J. Yamaoka,<sup>52</sup> T. Yamashita,<sup>40</sup> U.K. Yang<sup>k</sup>,<sup>14</sup> Y.C. Yang,<sup>28</sup> W.M. Yao,<sup>29</sup>  
 101 G.P. Yeh,<sup>18</sup> J. Yoh,<sup>18</sup> K. Yorita,<sup>14</sup> T. Yoshida,<sup>41</sup> G.B. Yu,<sup>49</sup> I. Yu,<sup>28</sup> S.S. Yu,<sup>18</sup> J.C. Yun,<sup>18</sup>  
 102 L. Zanello<sup>v</sup>,<sup>51</sup> A. Zanetti,<sup>54</sup> I. Zaw,<sup>23</sup> X. Zhang,<sup>25</sup> Y. Zheng<sup>b</sup>,<sup>9</sup> and S. Zucchelli<sup>t6</sup>

103 (CDF Collaboration\*)

104 <sup>1</sup>*Institute of Physics, Academia Sinica,*  
 105 *Taipei, Taiwan 11529, Republic of China*

106 <sup>2</sup>*Argonne National Laboratory, Argonne, Illinois 60439*

107 <sup>3</sup>*University of Athens, 157 71 Athens, Greece*

108 <sup>4</sup>*Institut de Fisica d'Altes Energies,*

109 *Universitat Autònoma de Barcelona,*

110 *E-08193, Bellaterra (Barcelona), Spain*

111 <sup>5</sup>*Baylor University, Waco, Texas 76798*

112 <sup>6</sup>*Istituto Nazionale di Fisica Nucleare Bologna,*

113 <sup>t</sup>*University of Bologna, I-40127 Bologna, Italy*

114 <sup>7</sup>*Brandeis University, Waltham, Massachusetts 02254*

115 <sup>8</sup>*University of California, Davis, Davis, California 95616*

116 <sup>9</sup>*University of California, Los Angeles, Los Angeles, California 90024*

117 <sup>10</sup>*University of California, San Diego, La Jolla, California 92093*

118 <sup>11</sup>*University of California, Santa Barbara, Santa Barbara, California 93106*

119 <sup>12</sup>*Instituto de Fisica de Cantabria, CSIC-University of Cantabria, 39005 Santander, Spain*

120 <sup>13</sup>*Carnegie Mellon University, Pittsburgh, PA 15213*

---

\* With visitors from <sup>a</sup>Universiteit Antwerpen, B-2610 Antwerp, Belgium, <sup>b</sup>Chinese Academy of Sciences, Beijing 100864, China, <sup>c</sup>University of Bristol, Bristol BS1 1TL, United Kingdom, <sup>d</sup>University of California Irvine, Irvine, CA 92697, <sup>e</sup>University of California Santa Cruz, Santa Cruz, CA 95064, <sup>f</sup>Cornell University, Ithaca, NY 14853, <sup>g</sup>University of Cyprus, Nicosia CY-1678, Cyprus, <sup>h</sup>University College Dublin, Dublin

121 <sup>14</sup>*Enrico Fermi Institute, University of Chicago, Chicago, Illinois 60637*  
122 <sup>15</sup>*Comenius University, 842 48 Bratislava,*  
123 *Slovakia; Institute of Experimental Physics, 040 01 Kosice, Slovakia*  
124 <sup>16</sup>*Joint Institute for Nuclear Research, RU-141980 Dubna, Russia*  
125 <sup>17</sup>*Duke University, Durham, North Carolina 27708*  
126 <sup>18</sup>*Fermi National Accelerator Laboratory, Batavia, Illinois 60510*  
127 <sup>19</sup>*University of Florida, Gainesville, Florida 32611*  
128 <sup>20</sup>*Laboratori Nazionali di Frascati, Istituto Nazionale*  
129 *di Fisica Nucleare, I-00044 Frascati, Italy*  
130 <sup>21</sup>*University of Geneva, CH-1211 Geneva 4, Switzerland*  
131 <sup>22</sup>*Glasgow University, Glasgow G12 8QQ, United Kingdom*  
132 <sup>23</sup>*Harvard University, Cambridge, Massachusetts 02138*  
133 <sup>24</sup>*Division of High Energy Physics, Department of Physics,*  
134 *University of Helsinki and Helsinki Institute of Physics, FIN-00014, Helsinki, Finland*  
135 <sup>25</sup>*University of Illinois, Urbana, Illinois 61801*  
136 <sup>26</sup>*The Johns Hopkins University, Baltimore, Maryland 21218*  
137 <sup>27</sup>*Institut für Experimentelle Kernphysik,*  
138 *Universität Karlsruhe, 76128 Karlsruhe, Germany*  
139 <sup>28</sup>*Center for High Energy Physics: Kyungpook National University,*  
140 *Daegu 702-701, Korea; Seoul National University, Seoul 151-742,*  
141 *Korea; Sungkyunkwan University, Suwon 440-746,*  
142 *Korea; Korea Institute of Science and Technology Information, Daejeon,*  
143 *305-806, Korea; Chonnam National University, Gwangju, 500-757, Korea*  
144 <sup>29</sup>*Ernest Orlando Lawrence Berkeley National Laboratory, Berkeley, California 94720*  
145 <sup>30</sup>*University of Liverpool, Liverpool L69 7ZE, United Kingdom*  
146 <sup>31</sup>*University College London, London WC1E 6BT, United Kingdom*  
147 <sup>32</sup>*Centro de Investigaciones Energeticas*  
148 *Medioambientales y Tecnologicas, E-28040 Madrid, Spain*  
149 <sup>33</sup>*Massachusetts Institute of Technology, Cambridge, Massachusetts 02139*  
150 <sup>34</sup>*Institute of Particle Physics: McGill University, Montréal,*  
151 *Canada H3A 2T8; and University of Toronto, Toronto, Canada M5S 1A7*  
152 <sup>35</sup>*University of Michigan, Ann Arbor, Michigan 48109*

- 153 <sup>36</sup>*Michigan State University, East Lansing, Michigan 48824*
- 154 <sup>37</sup>*University of New Mexico, Albuquerque, New Mexico 87131*
- 155 <sup>38</sup>*Northwestern University, Evanston, Illinois 60208*
- 156 <sup>39</sup>*The Ohio State University, Columbus, Ohio 43210*
- 157 <sup>40</sup>*Okayama University, Okayama 700-8530, Japan*
- 158 <sup>41</sup>*Osaka City University, Osaka 588, Japan*
- 159 <sup>42</sup>*University of Oxford, Oxford OX1 3RH, United Kingdom*
- 160 <sup>43</sup>*Istituto Nazionale di Fisica Nucleare, Sezione di Padova-Trento,*
- 161 <sup>u</sup>*University of Padova, I-35131 Padova, Italy*
- 162 <sup>44</sup>*LPNHE, Universite Pierre et Marie*
- 163 *Curie/IN2P3-CNRS, UMR7585, Paris, F-75252 France*
- 164 <sup>45</sup>*University of Pennsylvania, Philadelphia, Pennsylvania 19104*
- 165 <sup>46</sup>*Istituto Nazionale di Fisica Nucleare Pisa, <sup>q</sup>University of Pisa,*
- 166 <sup>r</sup>*University of Siena and <sup>s</sup>Scuola Normale Superiore, I-56127 Pisa, Italy*
- 167 <sup>47</sup>*University of Pittsburgh, Pittsburgh, Pennsylvania 15260*
- 168 <sup>48</sup>*Purdue University, West Lafayette, Indiana 47907*
- 169 <sup>49</sup>*University of Rochester, Rochester, New York 14627*
- 170 <sup>50</sup>*The Rockefeller University, New York, New York 10021*
- 171 <sup>51</sup>*Istituto Nazionale di Fisica Nucleare, Sezione di Roma 1,*
- 172 <sup>v</sup>*Sapienza Università di Roma, I-00185 Roma, Italy*
- 173 <sup>52</sup>*Rutgers University, Piscataway, New Jersey 08855*
- 174 <sup>53</sup>*Texas A&M University, College Station, Texas 77843*
- 175 <sup>54</sup>*Istituto Nazionale di Fisica Nucleare Trieste/ Udine,*
- 176 <sup>w</sup>*University of Trieste/ Udine, Italy*
- 177 <sup>55</sup>*University of Tsukuba, Tsukuba, Ibaraki 305, Japan*
- 178 <sup>56</sup>*Tufts University, Medford, Massachusetts 02155*
- 179 <sup>57</sup>*Waseda University, Tokyo 169, Japan*
- 180 <sup>58</sup>*Wayne State University, Detroit, Michigan 48201*
- 181 <sup>59</sup>*University of Wisconsin, Madison, Wisconsin 53706*
- 182 <sup>60</sup>*Yale University, New Haven, Connecticut 06520*

(Dated: March 24, 2008)

## Abstract

We present a search for standard model Higgs boson production in association with a  $W$  boson in proton-antiproton collisions ( $p\bar{p} \rightarrow W^\pm H \rightarrow \ell\nu b\bar{b}$ ) at a center of mass energy of 1.96 TeV. The search employs data collected with the CDF II detector which correspond to an integrated luminosity of approximately  $1 \text{ fb}^{-1}$ . We select events consistent with a signature of a single lepton ( $e^\pm/\mu^\pm$ ), missing transverse energy, and two jets. Jets corresponding to bottom quarks are identified with a secondary vertex tagging method and a neural network filter technique. The observed number of events and the dijet mass distributions are consistent with the standard model background expectations, and we set 95% confidence level upper limits on the production cross section times branching ratio ranging from 3.9 to 1.3 pb for Higgs boson masses from 110 to  $150 \text{ GeV}/c^2$ , respectively.

184 PACS numbers: 13.85.Rm, 14.80.Bn

185 **I. INTRODUCTION**

186 Standard electroweak theory predicts a single fundamental scalar particle, the Higgs  
 187 boson, which arises as a result of spontaneous electroweak symmetry breaking [1]; however,  
 188 the Higgs boson has not been direct observed experimentally. The current constraint on the  
 189 Higgs boson mass,  $m_H > 114.4 \text{ GeV}/c^2$  at 95% confidence level (C.L.), comes from direct  
 190 searches at LEP2 experiments [2]. Global fits to electroweak measurements exclude masses  
 191 above  $144 \text{ GeV}/c^2$  at 95% CL [3].

192 At the Tevatron  $p\bar{p}$  collider at Fermilab, the next-to-leading-order (NLO) Higgs boson  
 193 production cross section by gluon fusion is about ten times larger than for  $WH$  associated  
 194 production, and the cross section for  $WH$  is about twice that of  $ZH$  [4]. The Higgs boson  
 195 decay branching ratio is dominated by  $H \rightarrow b\bar{b}$  for  $m_H < 135 \text{ GeV}/c^2$  and by  $H \rightarrow W^+W^-$   
 196 for  $m_H > 135 \text{ GeV}/c^2$  [5]. Background QCD  $b\bar{b}$  production processes in the same invariant  
 197 mass range have cross sections at least four orders of magnitude greater than that of Higgs  
 198 boson production [6], and this renders searches in the  $gg \rightarrow H \rightarrow b\bar{b}$  channel extremely  
 199 difficult. However, requiring the leptonic decay of the associated weak boson reduces the  
 200 huge QCD background rate. As a result,  $WH \rightarrow \ell\nu b\bar{b}$  is considered to be one of the most  
 201 sensitive processes for low mass Higgs boson searches <sup>1</sup>.

202 Searches for  $WH \rightarrow \ell\nu b\bar{b}$  at  $\sqrt{s} = 1.96 \text{ TeV}$  have been most recently reported by CDF  
 203 (using data corresponding to an integrated luminosity of  $319 \text{ pb}^{-1}$ )[7] and D0 ( $440 \text{ pb}^{-1}$ )[8].  
 204 The CDF analysis used a secondary vertex  $b$ -tagging algorithm (SECVTX) to distinguish  $b$ -  
 205 quark jets from light flavor or gluon jets [9]. Upper limits on the Higgs boson production rate,  
 206 defined as the cross section times branching ratio ( $\sigma \cdot \mathcal{B}$ ), were derived for mass hypotheses  
 207 ranging from 110 to  $150 \text{ GeV}/c^2$ . The rate was constrained to be less than 10 pb at 95%  
 208 C.L. for  $m_H = 110$  and less than 2.8 pb for  $150 \text{ GeV}/c^2$ . In that analysis, about 50% of the  
 209 jets tagged by the SECVTX tagging algorithm were actually falsely  $b$ -tagged jets originating  
 210 from light flavor, gluon, or charm quarks. This effect is due to the finite resolution of track  
 211 measurements and the long lifetime of  $D$  mesons. Even the small fraction of mistagged  
 212 events in the dominant  $Wq\bar{q}$  process is significant compared to true  $Wb\bar{b}$  production. To  
 213 reduce this contamination and enhance the  $b$ -jet purity of our sample, we introduce a  $b$ -  
 214 tagging neural network filter which uses as inputs jet characteristics as well as secondary  
 215 vertex information.

---

<sup>1</sup> In this paper, lepton ( $\ell$ ) denotes electron ( $e^\pm$ ) or muon ( $\mu^\pm$ ), and neutrino ( $\nu$ ) denotes electron neutrino ( $e_\nu$ ) or muon neutrino ( $\mu_\nu$ ).



216 In this paper, we present a search for  $WH \rightarrow \ell\nu b\bar{b}$  production at CDF using about  $1 \text{ fb}^{-1}$   
 217 of data. Section II describes the CDF II detector. The event selection criteria are explained  
 218 in Sec. III. In Sec. IV, the  $b$ -tagging algorithm with SECVTX and neural network (NN) are  
 219 discussed in detail. Contributions from the standard model (SM) background are calculated  
 220 in Sec. V for various sources. In Sec. VI, signal acceptance and systematic uncertainties are  
 221 estimated. The search optimization and statistical interpretation of the results are presented  
 222 in Secs. VII and VIII, respectively. Finally, our conclusions are presented in Sec. IX.

## 223 II. CDF II DETECTOR

224 The CDF II detector geometry is described using a cylindrical coordinate system [10].  
 225 The  $z$ -axis follows the proton direction, and the polar angle  $\theta$  is usually expressed through  
 226 the pseudorapidity  $\eta = -\ln(\tan(\theta/2))$ . The detector is approximately symmetric in  $\eta$  and  
 227 in the azimuthal angle  $\phi$ .

228 Charged particles are tracked by a system of silicon microstrip detectors and a large open  
 229 cell drift chamber in the region  $|\eta| \leq 2.0$  and  $|\eta| \leq 1.0$ , respectively. The tracking detectors  
 230 are immersed in a 1.4 T solenoidal magnetic field aligned coaxially with the incoming beams,  
 231 allowing measurement of charged particle momentum transverse to the beamline.

232 The resolution on the transverse momentum  $p_T = p \sin \theta$  is measured to be  $\delta p_T/p_T \approx$   
 233  $0.1\% \cdot p_T(\text{GeV})$  for the combined tracking system. The resolution on the track impact  
 234 parameter ( $d_0$ ), or distance from the beamline axis to the track at the track's closest approach  
 235 in the transverse plane, is  $\sigma(d_0) \approx 40 \mu\text{m}$ , about  $30 \mu\text{m}$  of which is due to the transverse size  
 236 of the Tevatron interaction region.

237 Outside of the tracking systems and the solenoid, segmented calorimeters with projective  
 238 tower geometry are used to reconstruct electromagnetic showers and hadronic jets [11–13]  
 239 over the pseudo-rapidity range  $|\eta| < 3.6$ . A transverse energy  $E_T = E \sin \theta$  is measured in  
 240 each calorimeter tower where the polar angle ( $\theta$ ) is calculated using the measured  $z$  position  
 241 of the event vertex and the tower location.

242 Small contiguous groups of calorimeter towers with signals are identified and summed  
 243 together into an energy cluster. Electron candidates are identified in the central electromag-  
 244 netic calorimeter (CEM) as isolated, mostly electromagnetic clusters which match a track in  
 245 the pseudorapidity range  $|\eta| < 1.1$ . The electron transverse energy is reconstructed from the

246 electromagnetic cluster with a resolution  $\sigma(E_T)/E_T = 13.5\%/\sqrt{E_T/(\text{GeV})} \oplus 2\%$  [11]. Jets  
 247 are identified as a group of electromagnetic (EM) and hadronic (HAD) calorimeter clusters  
 248 which fall within a cone of radius  $\Delta R = \sqrt{\Delta\phi^2 + \Delta\eta^2} \leq 0.4$  units around a high- $E_T$  seed  
 249 cluster [14]. Jet energies are corrected for calorimeter non-linearity, losses in the gaps be-  
 250 tween towers, multiple primary interactions, out-of-cone losses, and inflow from underlying  
 251 event [15].

252 For this analysis, muons are detected in three separate subdetectors. After at least five  
 253 interaction lengths in the calorimeter, the muons first encounter four layers of planar drift  
 254 chambers (CMU), capable of detecting muons with  $p_T > 1.4 \text{ GeV}/c$  [16]. Four additional  
 255 layers of planar drift chambers (CMP) behind another 60 cm of steel detect muons with  
 256  $p_T > 2.8 \text{ GeV}/c$  [17]. These two systems cover the same central pseudorapidity region with  
 257  $|\eta| \leq 0.6$ . Muons which exit the calorimeters at  $0.6 \leq |\eta| \leq 1.0$  are tracked by the CMX  
 258 detector, consisting of four layers of drift chambers. Muon candidates are then identified as  
 259 isolated tracks which extrapolate to line segments or “stubs” in one of the muon subdetectors.  
 260 A track which is linked to both CMU and CMP stubs is called a CMUP muon.

261 The CDF trigger system is a three-level filter, with tracking information available even  
 262 at the first level [18]. Events used in this analysis have all passed the high-energy electron  
 263 or muon trigger selection. The first stage of the central electron trigger requires a track with  
 264  $p_T > 8 \text{ GeV}/c$  pointing to a tower with  $E_T > 8 \text{ GeV}$  and  $E_{\text{HAD}}/E_{\text{EM}} < 0.125$ . The first  
 265 stage of the muon trigger requires a track with  $p_T > 4 \text{ GeV}/c$  (CMUP) or  $8 \text{ GeV}/c$  (CMX)  
 266 pointing to a muon stub. A complete lepton reconstruction is performed online in the final  
 267 trigger stage, where we require  $E_T > 18 \text{ GeV}/c^2$  for electrons and  $p_T > 18 \text{ GeV}/c$  for muons.

### 268 III. EVENT SELECTION

269 The observable final state from the  $WH \rightarrow \ell\nu b\bar{b}$  signal consists of two jets plus a lepton  
 270 and missing transverse energy. The leptonic  $W$  decay requirement in  $WH$  events yields the  
 271 high- $p_T$  lepton and large missing transverse energy due to the neutrino.

272 The results presented here use data collected between February 2002 and February 2006.  
 273 The data collected using the CEM and CMUP triggers correspond to  $955 \pm 57 \text{ pb}^{-1}$ , while  
 274 the data from the CMX trigger corresponds to  $941 \pm 56 \text{ pb}^{-1}$ .

275 The missing transverse energy ( $\cancel{E}_T$ ) is a reconstructed quantity that is defined as the

276 opposite of the vector sum of all calorimeter tower energy depositions projected on the  
 277 transverse plane. It is often used as a measure of the sum of the transverse momenta of the  
 278 particles that escape detection, most notably neutrinos. To be more readily interpretable as  
 279 such, the raw  $\cancel{E}_T$  vector is adjusted for corrected jet energies, for the transverse momentum  
 280 of the muons, and for the energy deposition of any minimum ionizing high- $p_T$  muons.

281 Events are considered as  $WH$  candidates only if they have exactly one high- $p_T$  isolated  
 282 lepton [19], with  $E_T > 20$  GeV for electrons or  $p_T > 20$  GeV/ $c$  for muons. The isolation  
 283 cone of  $\Delta R = 0.4$  surrounding the lepton must have less than 10% of the lepton energy. A  
 284 primary event vertex position is calculated by fitting a subset of particle tracks which are  
 285 consistent with having come from the beamline. The distance between this primary event  
 286 vertex and the lepton track  $z_0$  must be less than 5 cm to ensure the lepton and the jets come  
 287 from the same hard interaction. Some leptonic  $Z$  decays would mimic the single-lepton  
 288 signature if a lepton is unidentified. Events are therefore rejected if a second track with  
 289  $p_T > 10$  GeV/ $c$  forms an invariant mass with the lepton which falls in the  $Z$ -boson mass  
 290 window ( $76 < m_{\ell X} < 106$  GeV/ $c^2$ ). The selected events are required to have  $\cancel{E}_T$  greater  
 291 than 20 GeV.

292 The  $WH$  signal includes two jets originating from  $H \rightarrow b\bar{b}$  decays; these jets are expected  
 293 to have large transverse energy. The jets are required to be in the pseudorapidity range  
 294 covered by the silicon detector so that secondary vertices from  $b$  decays can be reconstructed.  
 295 Specifically, we require the jets satisfy  $E_T > 15$  GeV and  $|\eta| < 2.0$ . The search for  $WH \rightarrow$   
 296  $\ell\nu b\bar{b}$  is performed in the sample of events with  $W+$  exactly 2 jets; however, samples of events  
 297 with  $W+1,3,\geq 4$  jets are used to cross-check the background modeling.

298 To increase the signal purity of the  $W+2$ -jet events, at least one jet must be  $b$ -tagged  
 299 by the SECVTX algorithm. If only one of the jets is  $b$ -tagged, the jet must also pass the  
 300 NN  $b$ -tagging filter. If there are two or more SECVTX  $b$ -tagged jets, the NN is not applied.  
 301 With a SECVTX mistag rate of 1%, it is rare that two or more jets in the same events are  
 302 mistagged by SECVTX.

#### 303 IV. SECONDARY VERTEX $b$ -TAGGING

304 Multijet final states have dominant contributions from QCD light flavor jet production,  
 305 but the standard model Higgs boson decays predominantly to bottom quark pairs. Correctly

306 identifying the  $b$  quark jets helps to remove most of the QCD background. An algorithm has  
 307 been developed and used to tag displaced secondary vertices from  $b$  quark decays; however,  
 308 the sample tagged by the SECVTX algorithm still has significant contamination from falsely-  
 309 tagged light-flavor or gluon jets and the misidentification of  $c$  quarks as  $b$ -jets [20]. This  
 310 search introduces a multivariate NN technique intended to improve the SECVTX tagging  
 311 purity.

312 The  $b$ -quark has a relatively long lifetime, and  $B$  hadrons formed during the hadroniza-  
 313 tion of the initial  $b$  quark can travel a significant distance on the order of millimeters before  
 314 decaying into a collection of lighter hadrons. The decay vertex can be reconstructed by iden-  
 315 tifying tracks which form a secondary vertex significantly displaced from the  $p\bar{p}$  interaction  
 316 point (primary vertex).

317 The SECVTX  $b$ -tagging algorithm is applied to each jet in the event, using only the tracks  
 318 which are within  $\eta$ - $\phi$  distance of  $\Delta R = 0.4$  of the jet direction. Displaced tracks in jets  
 319 are used for the SECVTX reconstruction and are distinguished by a large impact parameter  
 320 significance ( $|d_0/\sigma_{d_0}|$ ) where  $d_0$  and  $\sigma_{d_0}$  are the impact parameter and the total uncertainty  
 321 from tracking and beam position measurements. Secondary vertices are reconstructed with  
 322 a two-pass approach which tests for high-quality vertices in the first pass and allows lower-  
 323 quality vertices in the second pass. In pass 1, at least three tracks are required to pass  
 324 loose selection criteria ( $p_T > 0.5 \text{ GeV}/c$ ,  $|d_0/\sigma_{d_0}| > 2.0$ ), and a secondary vertex is fit  
 325 from the selected tracks. One of the tracks used in the reconstruction is required to have  
 326  $p_T > 1.0 \text{ GeV}/c$ . If pass 1 fails, then a vertex is sought in pass 2 from at least two tracks  
 327 satisfying tight selection criteria ( $p_T > 1.0 \text{ GeV}/c$ ,  $|d_0/\sigma_{d_0}| > 3.5$  and one of the pass 2 tracks  
 328 must have  $p_T > 1.5 \text{ GeV}/c$ ). If either pass is successful, the transverse distance ( $L_{xy}$ ) from  
 329 the primary vertex of the event is calculated along with the associated uncertainty. This  
 330 uncertainty  $\sigma_{L_{xy}}$  includes the uncertainty on the primary vertex position. Finally jets are  
 331 tagged positively or negatively depending on the  $L_{xy}$  significance ( $L_{xy}/\sigma_{L_{xy}}$ ):

$$332 \quad L_{xy}/\sigma_{L_{xy}} \geq 7.5 \quad (\text{positive tag}) \quad (1)$$

$$333 \quad L_{xy}/\sigma_{L_{xy}} \leq -7.5 \quad (\text{negative tag}) \quad (2)$$

334 These values have been tuned for optimum efficiency and purity in simulated  $b$ -jet samples  
 335 from decays of top quarks. The energy spectrum for those jets is similar to the spectrum  
 336 for  $b$  jets from decays of Higgs bosons.

337 The sign of  $L_{xy}$  indicates the position of the secondary vertex with respect to the primary  
 338 vertex along the direction of the jet. If the angle between the jet axis and the vector pointing  
 339 from the primary vertex to the secondary vertex is less than  $\pi/2$ ,  $L_{xy}$  is positively defined;  
 340 otherwise, it is negative. If  $L_{xy}$  is positive, the secondary vertex points towards the direction  
 341 of the jet, as in true  $B$  hadron decays. For negative  $L_{xy}$  the secondary vertex points away  
 342 from the jet; this may happen as a result of mismeasured tracks, so jets tagged with a  
 343 negative  $L_{xy}$  are labeled mistagged jets. In order to reject secondary vertices due to material  
 344 interaction, the algorithm vetoes two-track vertices found between 1.2 and 1.5 cm from the  
 345 center of the silicon detector (the inner radius of the beampipe and the outer radius of the  
 346 innermost silicon layer being within this range). All vertices more than 2.5 cm from the  
 347 center are rejected.

348 The negative tags are useful for evaluating the rate of false positive tags, which are defined  
 349 “mistags” in the background estimates. Mismeasurements are expected to occur randomly;  
 350 therefore the  $L_{xy}$  distribution of fake tags is expected to be symmetric with respect to zero.  
 351 Simulated events are used to correct a small asymmetry due to true long-lived particles in  
 352 light flavor jets.

353 The efficiency for identifying a secondary vertex is found to be different in the simulated  
 354 and observed datasets. We measure an efficiency scale factor, which is defined as the ratio  
 355 of the observed to the simulated efficiencies, to be  $0.91 \pm 0.06$  in a sample of high- $E_T$  jets  
 356 enriched in  $b$  jets by requiring a soft lepton ( $p_T > 8 \text{ GeV}/c^2$ ) from semileptonic heavy quark  
 357 decays [9].

358 Secondary vertex SECVTX  $b$ -tagging exploits the long lifetime of  $B$  hadrons.  $D$  hadrons  
 359 originating from  $c$ -quarks also have fairly long lifetime, and secondary vertices in  $c$ -jets are  
 360 frequently tagged. Therefore jets tagged by SECVTX are contaminated not only by falsely  
 361 tagged light flavor ( $uds$  or gluon) jets, but also by long-lived charmed hadrons in  $c$ -jets. A  
 362 neural network has been developed to filter the  $b$ -tagging results in order to improve the  
 363  $b$ -tagging purity.

364 The neural network used in this article employs the JETNET[21] package. The tagger is  
 365 designed with two networks in series. The  $b - l$  network is trained to separate  $b$ -jets from  
 366 light-quark jets ( $l$ -jets), and the  $b - c$  network is trained to separate  $b$ -jets from  $c$ -jets. Jets  
 367 which pass a cut on both of the NN outputs are accepted by the tagger. These neural  
 368 networks are trained and applied only to events which are already tagged by the SECVTX

369 algorithm. The current NN  $b$ -tagging is tuned to increase the purity of the SECVTX  $b$ -tagged  
 370 jets, not to increase the tagging efficiency.

371 The neural networks take as input the 16 variables listed in Table I. These variables  
 372 are chosen primarily because the  $b$ -quark jets have higher track multiplicity, larger invariant  
 373 mass, longer lifetime and a harder fragmentation function than  $c$ - and  $l$ -quarks jets. The  
 374 track parameters and  $L_{xy}$  significance are good discriminators for  $b$ -jets. The vertex  $p_T^{VTX}$   
 375 and invariant mass  $M_{VTX}$  are useful variables for identifying  $l$ -jets; however  $c$ -jets have  $p_T$   
 376 spectra similar to  $b$ -jets. Pseudo- $c\tau$  ( $L_{xy} \times M_{VTX}/p_T^{VTX}$ ), the vertex fit  $\chi^2$ , and the track-  
 377 based probability of a jet to come from the primary vertex are the best discriminators. The  
 378 outputs of the two neural networks are shown in Fig. 1.

379 The NN  $b$ -tagger is validated by comparing the performance on data and Monte Carlo  
 380 events. The NN output from  $b-l$  network on a sample of SECVTX tagged heavy-flavor  
 381 jets from events with an electron candidate with  $E_T > 8$  GeV electron data and from the  
 382 corresponding Monte Carlo sample are shown in Fig. 2, as are the outputs of the  $b-l$   
 383 network on tagged light-flavor jets from data and Monte Carlo<sup>2</sup>. Figure 2 shows the good  
 384 agreement in NN  $b$ -tagger performance between data and Monte Carlo.

385 We tune the cut value for 90%  $b$  efficiency (after the SECVTX efficiency), corresponding  
 386 to a value of  $NN_{b-l} = 0.182$  and  $NN_{b-c} = 0.242$ . The data-to-Monte-Carlo scale factor,  
 387 measured from the electron sample, is  $0.97 \pm 0.02$ . Note that this is an additional scale factor  
 388 with respect to the SECVTX efficiency scale factor because all of the jets under consideration  
 389 have already been tagged by SECVTX. At these cut values, the NN filter rejects 65% of  
 390 light-flavor jets and about 50% of the  $c$  jets while keeping 90% of  $b$ -jets after being tagged  
 391 by SECVTX.

## 392 V. BACKGROUND

393 The final state signature from  $WH \rightarrow \ell\nu b\bar{b}$  production can also be reached by other pro-  
 394 duction processes. The main background processes are  $W$ +jets production,  $t\bar{t}$  production,  
 395 and non- $W$  QCD multijet production. Several electroweak production processes also con-  
 396 tribute with smaller background rates. In the following subsections the contribution from  
 397 each background source is calculated in detail.

---

<sup>2</sup> A small but purified  $b$ -jet sample is obtained by requiring a soft lepton in the jet.

SECVTX variable	SECVTX-independent variable
Number of tracks in fitted vertex	Number of good tracks
Vertex fit $\chi^2$	Jet Probability [22]
Transverse decay length ( $L_{xy}$ )	Reconstructed mass of pass 1 tracks
$L_{xy}$ significance ( $L_{xy}/\sigma_{L_{xy}}$ )	Reconstructed mass of pass 2 tracks
Vertex Mass ( $M_{\text{vtx}} = \sqrt{(\sum  \mathbf{p}_{\text{vtx}} )^2 - (\sum \mathbf{p}_{\text{vtx}})^2}$ )	Number of pass 1 tracks
Pseudo- $c\tau$ ( $L_{xy} \times M_{\text{vtx}}/p_T^{\text{vtx}}$ )	Number of pass 2 tracks
$p_T^{\text{vtx}}/(\sum_{\text{good tracks}} p_T)$	$\sum_{\text{Pass1 track}} p_T/p_T^{\text{jet}}$
Vertex pass number (pass 1 or 2)	$\sum_{\text{Pass2 track}} p_T/p_T^{\text{jet}}$

TABLE I: Input variables used in the NN  $b$ -tagging filter. The variables in the first column are properties of the identified secondary vertex, while variables in the second column are jet properties independent of any identified vertex.

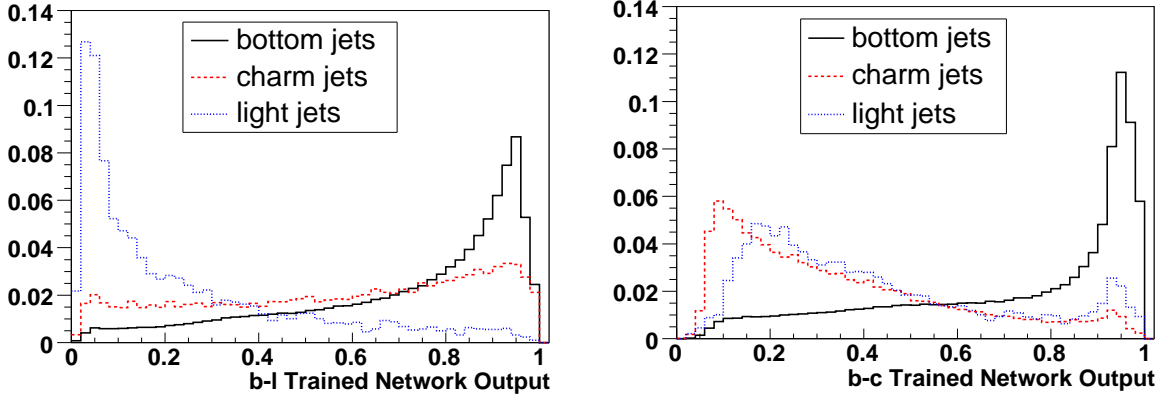


FIG. 1: Neural network outputs obtained from trainings of  $b$  vs.  $l$  jets (left) and  $b$  vs.  $c$  jets (right). Output distributions for  $b$ ,  $c$  and  $l$  jets are shown in solid, dashed, and dotted lines, respectively.

### 398 A. Non- $W$ QCD Multijet

399 Events from QCD multijet production sometimes mimic the  $W$ -boson signature with fake  
400 leptons or fake  $\cancel{E}_T$ . Non- $W$  leptons are reconstructed when a jet passes the lepton selection  
401 criteria or a heavy-flavor jet produces leptons via semileptonic decay. Non- $W$   $\cancel{E}_T$  can be  
402 observed via mismeasurements of energy or semileptonic decays of heavy-flavor quarks. It

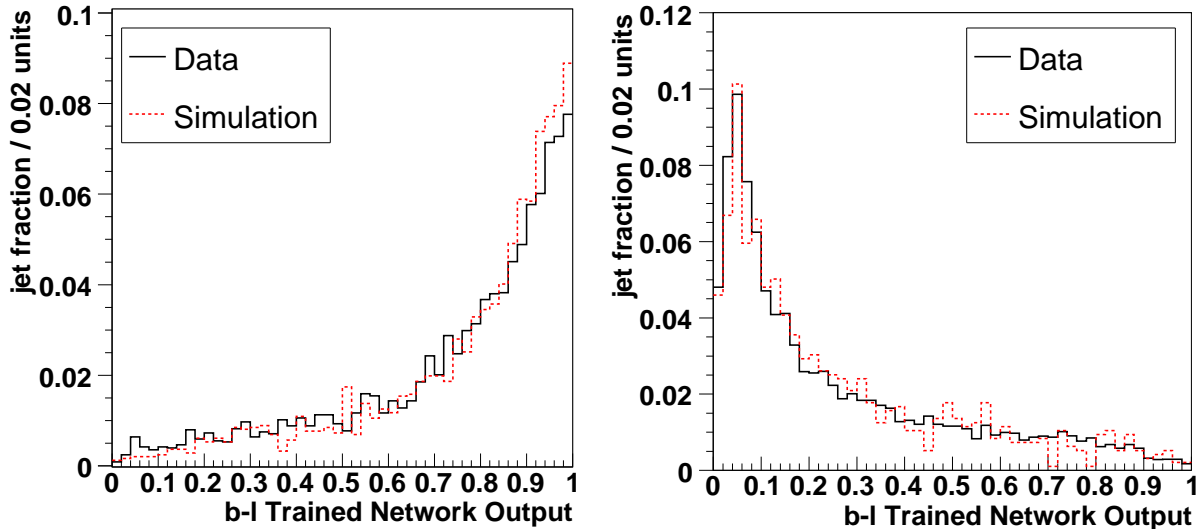


FIG. 2: Comparisons of NN  $b$ -tag output in data (solid line), and Monte Carlo (dashed line) for SECVTX-tagged heavy-flavor-enriched jets (left) and tagged light-flavor jets (right).

403 is difficult to model and produce the former class of events in detector simulation since  
 404 the reasons for mismeasurement are not known quantitatively. Instead, we estimate the  
 405 contribution of non- $W$  events directly from the data sample before  $b$ -tagging is applied.

406 Generally, the bulk of non- $W$  events are characterized by a non-isolated lepton and small  
 407  $\cancel{E}_T$ . Lepton isolation  $I$  is defined as the ratio of calorimeter energy inside a cone of  $\Delta R = 0.4$   
 408 about the lepton to the lepton energy itself. The quantity  $I$  is small if the lepton is well-  
 409 isolated from the rest of the event, as typified by a true leptonic  $W$  decay. This feature is  
 410 used to extrapolate the expected non- $W$  contribution into our signal region, namely, small  
 411  $I$  and large  $\cancel{E}_T$ . The following 4 sideband sectors are used for the extrapolation:  $I > 0.2$   
 412 and  $\cancel{E}_T < 15$  GeV (region A),  $I < 0.1$  and  $\cancel{E}_T < 15$  GeV (region B),  $I > 0.2$  and  $\cancel{E}_T > 20$   
 413 GeV (region C), and  $I < 0.1$  and  $\cancel{E}_T > 20$  GeV (region D). Here, region D corresponds to  
 414 the signal region. In extracting the non- $W$  background contribution from data, we make  
 415 the following two assumptions: lepton isolation and  $\cancel{E}_T$  are uncorrelated in non- $W$  events,  
 416 and the  $b$ -tagging rate is not dependent on  $\cancel{E}_T$  in non- $W$  events. The level at which these  
 417 assumptions are justified determines the assigned uncertainty.

418 With the first assumption, the number of non- $W$  events ( $N_D^{\text{non-}W}$ ) and their relative



419 fraction in the signal region before requiring  $b$ -tagging ( $f_{\text{non-}W}$ ) obey the following relations:

$$420 \quad N_D^{\text{non-}W} = \frac{N_B \times N_C}{N_A}, \quad (3)$$

$$421 \quad f_{\text{non-}W} = \frac{N_D^{\text{non-}W}}{N_D} = \frac{N_B \times N_C}{N_A \times N_D}, \quad (4)$$

422 where  $N_i$  ( $i = A, B, C, D$ ) are the number of pretag events in each sideband region. The  
 423 number of pretag events has been corrected for known sources of prompt leptons. By in-  
 424 voking the second assumption, the SECVTX  $b$ -tagging efficiency obtained in region  $B$  can be  
 425 applied to the signal region  $D$ . Here we define an event tagging efficiency per taggable jet  
 426 (one with at least two good SECVTX tracks) as follows:

$$427 \quad r_B = \frac{N_B^{(\text{tagged event})}}{N_B^{(\text{taggable jet})}}, \quad (5)$$

428 where  $N_B^{(\text{tagged event})}$  and  $N_B^{(\text{taggable jet})}$  are the number of tagged events and taggable jets in  
 429 region  $B$ , respectively. Then the number of non- $W$  background in region  $D$  after SECVTX  
 430  $b$ -tagging ( $N_D^{+\text{non-}W}$ ) is obtained by using the ‘‘Tag Rate’’ relation:

$$431 \quad N_D^{+\text{non-}W} = f_{\text{non-}W} \times r_B \times N_D^{(\text{taggable jets})}. \quad (6)$$

432 It is also possible to estimate non- $W$  contribution solely from the SECVTX-tagged sample  
 433 as:

$$434 \quad N_D^{+\text{non-}W} = \frac{N_B^+ \times N_C^+}{N_A^+}, \quad (7)$$

435 where  $N_X^+$  ( $X = A, B, C, D$ ) in the ‘‘Tagged Method’’ are the number of events with positive  
 436 tags. These methods are data-based techniques, so the estimates could also contain other  
 437 background processes. The contributions from  $t\bar{t}$  and  $W$ +jets events to each sideband region  
 438 are subtracted according to the calculated cross sections for those processes, including the  
 439 appropriate tagging efficiencies.

440 To validate the four-sector method and estimate their systematic uncertainties, we vary  
 441 the boundaries of the four regions and divide the  $I$  and  $\cancel{E}_T$  sidebands into two E ( $0.1 <$   
 442  $I < 0.2$  and  $\cancel{E}_T > 20$  GeV) and F ( $I < 0.1$  and  $15 < \cancel{E}_T < 20$  GeV) sidebands. The observed  
 443 deviations imply a 25% systematic uncertainty in the non- $W$  background yield, assigned  
 444 conservatively for both the pretag and tagged estimates.

445 The independent estimates from the tag rate method (Eq. 6) and the tagged method  
 446 (Eq. 7) are combined using a weighted average. The result from the tagged method gives a

447 slightly higher estimate than the tag rate method, but the two results are consistent within  
448 the 25% uncertainty.

449 A non- $W$  rejection factor associated with the NN  $b$ -tagging filter is measured from data  
450 in region  $C$ . Region  $C$  has event kinematics similar to non- $W$  events in the signal region  $D$   
451 because lepton isolation is the only difference between the two regions. The non- $W$  estimate  
452 calculated before applying NN  $b$ -tagging is scaled by this NN rejection factor; this assumes  
453 the NN filter is uncorrelated with the isolation.

454 The non- $W$  estimate for events with at least two SECVTX tags is obtained by measuring  
455 the ratio of the number of events with at least one  $b$ -tag to the number with at least two  
456  $b$ -tags in sideband regions and applying the ratio to the estimate of tagged non- $W$  events in  
457 the signal region  $D$ .

## 458 **B. Mistagged Jets**

459 The rate at which SECVTX falsely tags light-flavor jets is derived from generic jet samples  
460 in varying bins of  $\eta$ ,  $\phi$ , jet  $E_T$ , track multiplicity, and total event  $E_T$  scalar sum. Tag rate  
461 probabilities are summed for all of the taggable jets in the event, jets with at least two tracks  
462 well measured in the silicon detector. Since the double-mistag rate is small, this sum is a  
463 good approximation of the single-tag event rate. Negative mistags – tags with unphysical  
464 negative decay length due to finite tracking resolution – are assumed to be a good estimate  
465 of falsely tagged jets, independent to first order of heavy flavor content in the generic jet  
466 sample. The systematic uncertainty on the rate is largely due to self-consistency in the  
467 parameterization as applied to the generic jet sample. The positive mistag rate is enhanced  
468 relative to the negative tag rate by light-flavor secondary vertices and material interactions  
469 in the silicon detectors. As a result, the positive mistag rate is corrected by multiplying  
470 the negative mistag rate by a factor of  $1.37 \pm 0.15$ . This factor is measured in a control  
471 sample by fitting the asymmetry in the vertex mass distribution of positive tags over negative  
472 tags [23]. An additional correction factor of  $1.05 \pm 0.03$  is applied for data collected after  
473 December 2004, when the Tevatron beam position changed slightly. The mistag rate per jet  
474 is applied to events in the  $W$ +jets sample. The total estimate is corrected for the non- $W$   
475 QCD fraction and also the top quark contributions to the pretag sample. To estimate the  
476 mistag contribution in NN-tagged events, we apply the light flavor rejection power of the

477 NN filter  $0.35 \pm 0.05$  as measured using light-flavor jets from various data and simulated  
 478 samples.

### 479 C. $W$ +Heavy Flavor

480 The  $Wb\bar{b}$ ,  $Wc\bar{c}$ , and  $Wc$  states are major background sources of secondary vertex tags.  
 481 Large theoretical uncertainties exist for the overall normalization in part because current  
 482 Monte Carlo programs generate  $W$ +heavy-flavor events only to leading order. Consequently,  
 483 rates for these processes are normalized to data. The contribution from true heavy-flavor  
 484 production in  $W$ +jet events is determined from measurements of the heavy-flavor event  
 485 fraction in  $W$ +jet events and the  $b$ -tagging efficiency for those events, as explained below.

486 The fraction of  $W$ +jets events produced with heavy-flavor jets has been studied exten-  
 487 sively using an ALPGEN + HERWIG combination of Monte Carlo programs [24, 25]. Calcula-  
 488 tions of the heavy-flavor fraction in ALPGEN have been calibrated using a jet data sample,  
 489 and measurements indicate a scaling factor of  $1.5 \pm 0.4$  is necessary to make the heavy-flavor  
 490 production in Monte Carlo match the production in multijet data [9]. The final results of  
 491 heavy-flavor fractions are obtained as shown in Table II. In the table, 1B and 1C refer to the  
 492 case in which only one of the heavy-flavor jets is detected; this happens when one jet goes  
 493 out of the detector coverage or when two parton jets merge into the same reconstructed jet.  
 494 Similarly, 2B and 2C refer to the case in which both of the heavy-flavor jets are observed.

495 For the tagged  $W$ +heavy flavor background estimate, the heavy-flavor fractions and  
 496 tagging rates given in Tables II and III are multiplied by the number of pretag  $W$ +jets  
 497 candidate events in data, after correction for the contribution of non- $W$  and  $t\bar{t}$  events to the  
 498 pretag sample.

499 The previous CDF analysis using  $319 \text{ pb}^{-1}$  of data provided some evidence that the  
 500 disagreement between the predicted and observed numbers of  $W$ +1 jet and  $W$ +2 jet events is  
 501 due to the heavy-flavor fraction [7]. In this analysis, an updated correction factor of  $1.2 \pm 0.2$ ,  
 502 obtained by fitting tagged  $W$ +1 jet events only, is applied to the heavy-flavor fraction. The  
 503  $W$ + heavy flavor background contribution is obtained by the following relation:

$$504 \quad N_{W+HF} = f_{HF} \cdot \epsilon_{\text{tag}} \cdot [N_{\text{pretag}} \cdot (1 - f_{\text{non-}W}) - N_{\text{TOP}} - N_{\text{EWK}}], \quad (8)$$

505 where  $f_{HF}$  is the heavy-flavor fraction,  $\epsilon_{\text{tag}}$  is the tagging efficiency,  $N_{\text{TOP}}$  is the expected

Jet Multiplicity	1 jet	2 jets	3 jets	$\geq 4$ jets
$Wb\bar{b}$ (1B) (%)	$1.0 \pm 0.3$	$1.4 \pm 0.4$	$2.0 \pm 0.5$	$2.2 \pm 0.6$
$Wb\bar{b}$ (2B) (%)	-	$1.4 \pm 0.4$	$2.0 \pm 0.5$	$2.6 \pm 0.7$
$Wc\bar{c}$ (1C) (%)	$1.6 \pm 0.4$	$2.4 \pm 0.6$	$3.4 \pm 0.9$	$3.6 \pm 1.0$
$Wc\bar{c}$ (2C) (%)	-	$1.8 \pm 0.5$	$2.7 \pm 0.7$	$3.7 \pm 1.0$
$Wc$ (%)	$4.3 \pm 0.9$	$6.0 \pm 1.3$	$6.3 \pm 1.3$	$6.1 \pm 1.3$

TABLE II: The heavy-flavor fractions, given in percent, for the  $W + \text{jets}$  sample. The results from ALPGEN Monte Carlo have been scaled by the data-derived calibration factor of  $1.5 \pm 0.4$ . ( $Wc$  fractions have not been rescaled.)

506 number of  $t\bar{t}$  and single top events, and  $N_{\text{EWK}}$  is the expected number of  $WW$ ,  $WZ$ , and  $Z$   
507 boson events.

#### 508 D. Top and Electroweak Backgrounds

509 Production of both single top quark and top-quark pairs contribute to the tagged lep-  
510 ton+jets sample. Several electroweak boson production processes also contribute.  $WW$   
511 pairs can decay to a lepton, neutrino as missing energy, and two jets, one of which may be  
512 charm.  $WZ$  events can decay to the signal  $Wb\bar{b}$  or  $Wc\bar{c}$  final state. Finally,  $Z \rightarrow \tau^+\tau^-$   
513 events can have one leptonic  $\tau$  decay and one hadronic decay. The leptonic  $\tau$  decay gives  
514 rise to a lepton + missing transverse energy, while the hadronic decay yields a narrow jet of  
515 hadrons with a non-zero lifetime.

516 The normalization of the diboson and single top backgrounds are based on the theoretical  
517 cross sections listed in Table IV, the luminosity, and the acceptance and  $b$ -tagging efficiency  
518 derived from Monte Carlo events [19, 26–28]. The acceptance is corrected for lepton identi-  
519 fication, trigger efficiencies, and the  $z$  vertex cut. The tagging efficiency is always corrected  
520 by the  $b$ -tagging scale factor.

Jet Multiplicity	1 jet	2 jets	3 jets	$\geq 4$ jets
$\geq 1$ SECVTX $b$ -tag (%)				
$Wb\bar{b}$ (1B)	$33.2 \pm 2.4$	$34.5 \pm 2.5$	$36.7 \pm 2.6$	$40.2 \pm 2.9$
$Wb\bar{b}$ (2B)	-	$51.3 \pm 3.6$	$54.1 \pm 3.8$	$55.1 \pm 3.9$
$Wc\bar{c}$ (1C)	$6.2 \pm 0.9$	$8.0 \pm 1.1$	$9.7 \pm 1.4$	$11.6 \pm 1.6$
$Wc\bar{c}$ (2C)	-	$14.4 \pm 2.0$	$17.0 \pm 2.4$	$17.8 \pm 2.5$
$Wc$	$8.9 \pm 1.3$	$8.7 \pm 1.2$	$7.6 \pm 1.1$	$3.4 \pm 0.5$
$\geq 1$ SECVTX and NN $b$ -tag (%)				
$Wb\bar{b}$ (1B)	$29.9 \pm 2.1$	$31.8 \pm 2.3$	$34.1 \pm 2.4$	$35.9 \pm 2.6$
$Wb\bar{b}$ (2B)	-	$47.2 \pm 3.4$	$51.5 \pm 3.7$	$51.3 \pm 3.6$
$Wc\bar{c}$ (1C)	$3.8 \pm 0.5$	$5.5 \pm 0.8$	$6.1 \pm 0.9$	$6.4 \pm 0.9$
$Wc\bar{c}$ (2C)	-	$9.9 \pm 1.4$	$8.6 \pm 1.2$	$9.5 \pm 1.4$
$Wc$	$5.0 \pm 0.7$	$4.6 \pm 0.7$	$3.1 \pm 0.4$	$3.4 \pm 0.5$
$\geq 2$ SECVTX $b$ -tag (%)				
$Wb\bar{b}$ (2B)	-	$9.7 \pm 0.7$	$13.6 \pm 1.0$	$11.5 \pm 0.8$
$Wc\bar{c}$ (2C)	-	$1.2 \pm 0.2$	$0.8 \pm 0.1$	$0.9 \pm 0.1$

TABLE III: The  $b$ -tagging efficiencies in percent for various  $b$ -tagging strategies on individual  $W$ +heavy-flavor processes. Categories 1B, 2B refer to number of taggable  $b$ -jets in the events, with similar categories for charm jets. Those numbers include the effect of the data-to-Monte Carlo scale factors algorithm and the neural network filter.

## E. Summary of Background Estimate

We have described the contributions of individual background sources to the final background estimate. The background estimates for the condition of exactly one  $b$ -tagged jet after applying the NN filter and at least two SECVTX  $b$ -tagged jets are summarized in Tables V and VI. The estimates are plotted in Figs. 3 and 4 for the case of exactly one  $b$ -tag before and after applying the NN  $b$ -tag filter. The observed number of events in the data and the SM background expectations are consistent both before and after NN  $b$ -tagging is applied. The same is true for the number of events with at least two  $b$ -tagged jets. (See

Theoretical Cross Sections	
$WW$	$12.40 \pm 0.80$ pb
$WZ$	$3.96 \pm 0.06$ pb
$ZZ$	$1.58 \pm 0.02$ pb
Single top $s$ -channel	$0.88 \pm 0.05$ pb
Single top $t$ -channel	$1.98 \pm 0.08$ pb
$Z \rightarrow \tau^+\tau^-$	$320 \pm 9$ pb
$t\bar{t}$	$6.7^{+0.7}_{-0.9}$ pb

TABLE IV: Theoretical cross sections and uncertainties for the electroweak and single top backgrounds, along with the theoretical cross section for  $t\bar{t}$  at  $m_t = 175 \text{ GeV}/c^2$ . The cross section of  $Z^0 \rightarrow \tau^+\tau^-$  is obtained in the dilepton mass range  $m_{\tau\tau} > 30 \text{ GeV}/c^2$  together with a  $k$ -factor (NLO/LO) of 1.4.

529 Table VI and Fig. 4.)

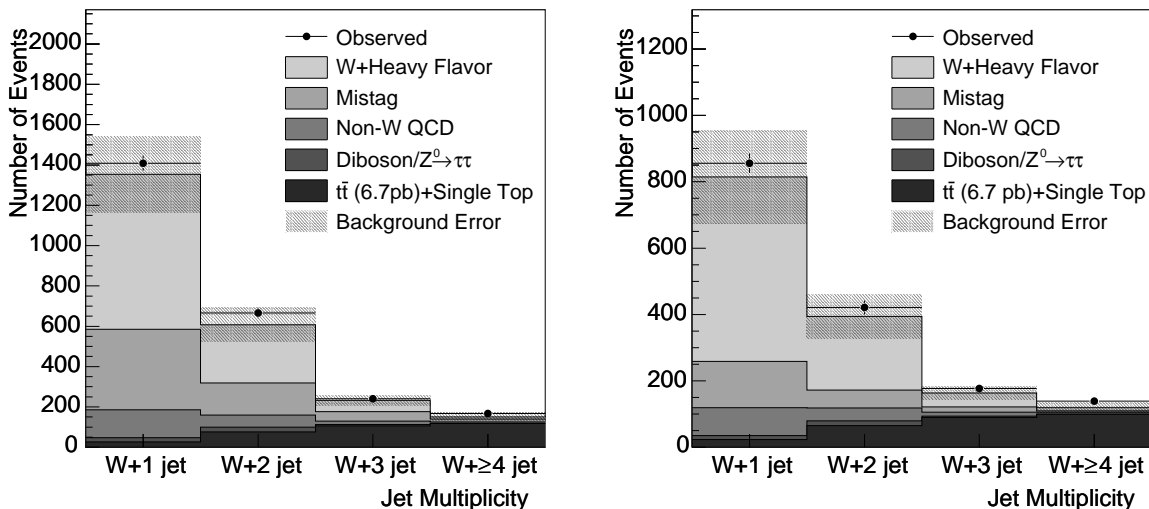


FIG. 3: Number of events as a function of jet multiplicity for events with exactly one SECVTX  $b$ -tag before(left) and after(right) applying the NN  $b$ -tagging requirement.

Jet Multiplicity	1 jet	2 jets	3 jets	$\geq 4$ jets
Pretag Events	94051	14604	2362	646
Mistag	$139.7 \pm 27.3$	$53.9 \pm 10.7$	$15.7 \pm 3.1$	$4.2 \pm 0.8$
$Wb\bar{b}$	$306.9 \pm 106.9$	$144.7 \pm 49.4$	$29.9 \pm 9.7$	$6.4 \pm 2.5$
$Wc\bar{c}$	$63.1 \pm 22.0$	$43.0 \pm 14.7$	$8.7 \pm 2.8$	$1.9 \pm 0.8$
$Wc$	$185.7 \pm 47.2$	$34.4 \pm 9.0$	$3.4 \pm 0.9$	$0.6 \pm 0.2$
$t\bar{t}(6.7\text{pb})$	$6.9 \pm 1.2$	$42.0 \pm 6.6$	$84.9 \pm 12.8$	$98.6 \pm 14.3$
Single Top	$16.7 \pm 1.8$	$23.5 \pm 2.4$	$4.8 \pm 0.5$	$0.8 \pm 0.1$
Diboson/ $Z^0 \rightarrow \tau^+\tau^-$	$11.7 \pm 2.2$	$14.2 \pm 2.3$	$3.9 \pm 0.9$	$1.0 \pm 0.3$
non- $W$ QCD	$84.2 \pm 14.1$	$38.9 \pm 6.7$	$12.1 \pm 2.3$	$5.5 \pm 1.2$
Total Background	$814.9 \pm 140.7$	$394.4 \pm 66.6$	$163.4 \pm 18.7$	$118.9 \pm 14.9$
Observed Events	856	421	177	139

TABLE V: Background estimate for events with exactly one SECVTX  $b$ -tag that passes the NN filter as a function of jet multiplicity.

Jet Multiplicity	2 jets	3 jets	$\geq 4$ jets
Observed Events(pretag)	14604	2362	646
Mistag	$3.5 \pm 0.5$	$2.0 \pm 0.3$	$1.2 \pm 0.2$
$Wb\bar{b}$	$20.3 \pm 7.0$	$5.7 \pm 1.8$	$1.0 \pm 0.4$
$Wc\bar{c}$	$3.3 \pm 1.1$	$0.4 \pm 0.1$	$0.1 \pm 0.04$
$Wc$	-	-	-
$t\bar{t} (6.7\text{pb})$	$10.4 \pm 2.3$	$29.5 \pm 6.4$	$45.5 \pm 9.9$
Single Top	$4.2 \pm 0.7$	$1.4 \pm 0.2$	$0.3 \pm 0.1$
Diboson/ $Z^0 \rightarrow \tau^+\tau^-$	$1.2 \pm 0.3$	$0.3 \pm 0.1$	$0.1 \pm 0.1$
non- $W$ QCD	$1.4 \pm 0.3$	$0.9 \pm 0.2$	$0.3 \pm 0.1$
Total Background	$44.2 \pm 8.5$	$40.1 \pm 6.8$	$48.6 \pm 10.0$
Observed Events	39	44	65

TABLE VI: Background estimate for events with at least two SECVTX  $b$ -tagged jets as a function of jet multiplicity.

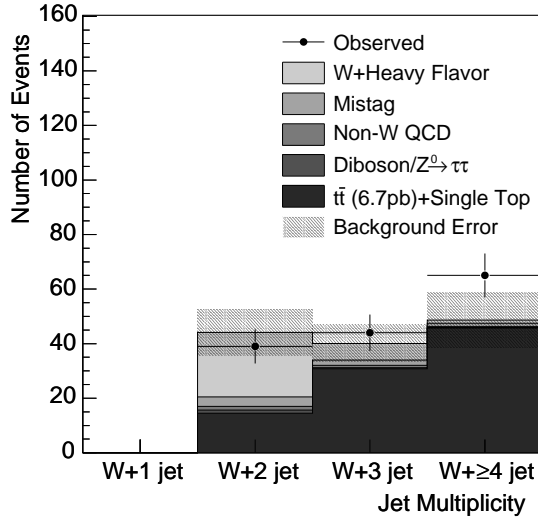


FIG. 4: Number of events as a function of jet multiplicity for events with at least two SECVTX  $b$ -tagged jets.

## 530 VI. HIGGS BOSON SIGNAL ACCEPTANCE

531 The kinematics of the SM  $WH \rightarrow \ell\nu b\bar{b}$  process are well defined, and events can be  
 532 simulated accurately by Monte Carlo programs. The PYTHIA program was used to generate  
 533 the signal samples [29]. Only Higgs boson masses between 110 and 150 GeV/ $c^2$  are considered  
 534 because this is the mass region for which the decay  $H \rightarrow b\bar{b}$  dominates. The number of  
 535 expected  $WH \rightarrow \ell\nu b\bar{b}$  events  $N$  is given by:

$$536 \quad N = \epsilon \cdot \int \mathcal{L} dt \cdot \sigma(p\bar{p} \rightarrow WH) \cdot \mathcal{B}(H \rightarrow b\bar{b}), \quad (9)$$

537 where  $\epsilon$ ,  $\int \mathcal{L} dt$ ,  $\sigma(p\bar{p} \rightarrow WH)$ , and  $\mathcal{B}(H \rightarrow b\bar{b})$  are the event detection efficiency, integrated  
 538 luminosity, production cross section, and branching ratio, respectively. The production cross  
 539 section and branching ratio are calculated to NLO precision [5]. The acceptance  $\epsilon$  is broken  
 540 down into the following factors:

$$541 \quad \epsilon = \sum_{\ell=e,\mu,\tau} (\epsilon_{z_0} \cdot \epsilon_{\text{trigger}} \cdot \epsilon_{\text{lepton ID}} \cdot \epsilon_{b\text{tag}} \cdot \epsilon_{\text{kinematics}} \cdot \mathcal{B}(W \rightarrow \ell\nu)), \quad (10)$$

542 where  $\epsilon_{z_0}$ ,  $\epsilon_{\text{trigger}}$ ,  $\epsilon_{\text{lepton ID}}$ ,  $\epsilon_{b\text{tag}}$ , and  $\epsilon_{\text{kinematics}}$  are efficiencies to meet the requirements of  
 543 primary vertex, trigger, lepton identification,  $b$ -tagging, and kinematics. The major sources  
 544 of inefficiency are the lepton identification, jet kinematics, and  $b$ -tagging factors; each is



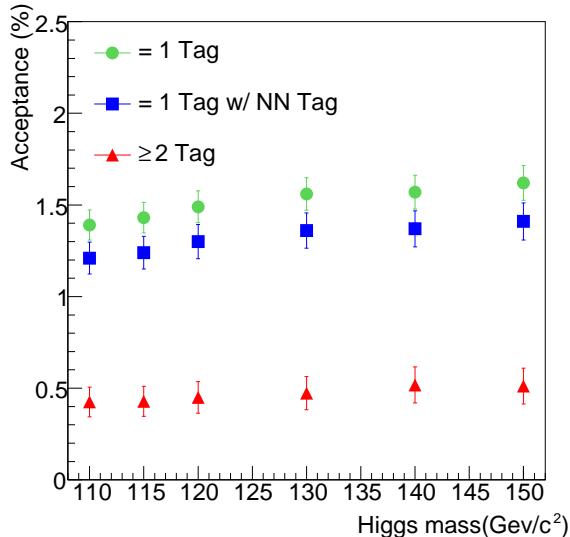


FIG. 5: The summary of acceptance of the process  $WH \rightarrow \ell\nu b\bar{b}$  in W+2jet bin for various  $b$ -tagging strategies as a function of Higgs boson mass.

545 a factor between 0.3 and 0.45. The factor  $\epsilon_{z_0}$  is obtained from data, and the others are  
 546 calculated using Monte Carlo samples. The total signal acceptances for various  $b$ -tagging  
 547 options including all systematic uncertainties as a function of Higgs boson mass are shown  
 548 in Fig. 5.

549 The expected number of signal events is estimated by Eq. 9 at each Higgs boson mass  
 550 point. The expectations for various  $b$ -tagging strategies are shown in Table VII. The NN  
 551  $b$ -tagging filter keeps about 90% of signal while it removes 35% of the total background in  
 552 W+2 jet events as shown in Fig. 3.

553 The total systematic uncertainty on the acceptance stems from the jet energy scale, ini-  
 554 tial and final state radiation, lepton identification, trigger efficiencies, and  $b$ -tagging. A 2%  
 555 uncertainty on the lepton identification efficiency is assigned for each lepton type (CEM elec-  
 556 tron, CMUP and CMX muon), based on studies of  $Z$  boson events. For each of the high  $p_T$   
 557 lepton triggers, a 1% uncertainty is measured from backup trigger paths or  $Z$  boson events.  
 558 The initial and final state radiation systematic uncertainties are estimated by changing the  
 559 parameters related to ISR and FSR from nominal values to half or double the nominal [30].  
 560 The difference from the nominal acceptance is taken as the systematic uncertainty. The  
 561 uncertainty in the incoming parton energies relies on the eigenvalue uncertainties provided  
 562 in the PDF fits. An NLO version of the PDFs, CTEQ6M, provides a 90% confidence interval

Higgs Mass (GeV/ $c^2$ )	Expected Signal Events			
	Pretag	1 tag	1 tag with NNtag	$\geq 2$ tag
110	4.81 $\pm$ 0.34	2.15 $\pm$ 0.18	1.87 $\pm$ 0.18	0.66 $\pm$ 0.13
115	3.99 $\pm$ 0.28	1.80 $\pm$ 0.15	1.56 $\pm$ 0.15	0.54 $\pm$ 0.11
120	3.23 $\pm$ 0.23	1.45 $\pm$ 0.12	1.26 $\pm$ 0.12	0.44 $\pm$ 0.09
130	2.05 $\pm$ 0.15	0.93 $\pm$ 0.08	0.81 $\pm$ 0.08	0.28 $\pm$ 0.06
140	1.03 $\pm$ 0.07	0.46 $\pm$ 0.04	0.40 $\pm$ 0.04	0.15 $\pm$ 0.03
150	0.40 $\pm$ 0.03	0.18 $\pm$ 0.02	0.16 $\pm$ 0.02	0.06 $\pm$ 0.01

TABLE VII: Expected number of  $WH \rightarrow \ell\nu b\bar{b}$  signal events with systematic uncertainties for various  $b$ -tagging options, where “tag” and “NNtag” stand for SECVTX  $b$ -tagging and NN  $b$ -tagging, respectively.

of each eigenvector [31]. The nominal PDF value is reweighted to the 90% confidence level value, and the corresponding reweighted acceptance is computed. The differences between nominal and reweighted acceptances are added in quadrature, and the total is assigned as the systematic uncertainty [9].

The uncertainty due to the jet energy scale uncertainty (JES) [15] is calculated by shifting jet energies in  $WH$  Monte Carlo samples by  $\pm 1\sigma$ . The deviation from the nominal acceptance is taken as the systematic uncertainty. The systematic uncertainty on the SECVTX  $b$ -tagging efficiency is based on the scale factor uncertainty discussed in Sec. IV. When NN  $b$ -tagging is applied, the scale factor uncertainty is added to that of SECVTX in quadrature. The total systematic uncertainties for various  $b$ -tagging options are summarized in Table VIII.

## VII. OPTIMIZATION OF SEARCH STRATEGIES

The search strategy is optimized by calculating a signal significance defined as  $S/\sqrt{B}$ , where  $S$  and  $B$  are the number of expected signal and background events. In this analysis,  $S$  and  $B$  are counted within a window which gives the best significance in dijet mass distribution for the particular Higgs mass hypothesis being considered. The window itself is optimized by varying the window peak and width for each  $b$ -tagging strategy. A comparison

source	uncertainty (%)		
	1 Tag	1 Tag & NNtag	$\geq 2$ Tag
Lepton ID	2.0%	2.0%	2.0%
Trigger	<1%	<1%	<1%
ISR	1.5%	1.8%	4.3%
FSR	2.8%	3.2%	8.6%
PDF	1.6%	1.7%	2.0%
JES	2.3%	2.3%	3.0%
<i>b</i> -tagging	3.8%	5.3%	16%
Total	5.8%	7.2%	19%

TABLE VIII: Systematic uncertainties for various *b*-tagging requirements. The labels “Tag” and “NNtag” refer to SECVTX and NN *b*-tagging, respectively.

580 of the significance for various *b*-tagging options, shown in Fig. 6, provides an *a priori* metric  
581 that predicts which selection gives the best result.

582 Requiring the NN filter improves the sensitivity by about 10% in the sample of events  
583 with exactly one *b* tag. The significance in double-tagged events is almost the same as  
584 that in events with at least one tag and no NN filter. Combining the two results therefore  
585 yields another sensitivity improvement. This combined use of two separate *b*-tagged samples  
586 provides a significant improvement as shown in Fig. 6. The total significance increases by  
587 20% moving from “ $\geq 1$  tag” to separate categories “1 tag w/ NNTag” and “ $\geq 2$  Tag.”  
588 Therefore, we quote final results from events having exactly one SECVTX *b*-tagged jet passing  
589 the neural network filter or at least two SECVTX *b*-tagged jets.

## 590 VIII. LIMIT ON HIGGS BOSON PRODUCTION RATE

591 As shown in section VII, there is no significant excess number of events over the SM  
592 background expectation. Because the dijet mass resonance is a useful discriminant for the  
593 Higgs boson signature, we use a binned likelihood technique to fit the observed dijet mass  
594 distributions in Figs. 7 and 8, and set an upper limit on the *WH* production cross section  
595 times  $H \rightarrow b\bar{b}$  branching ratio.

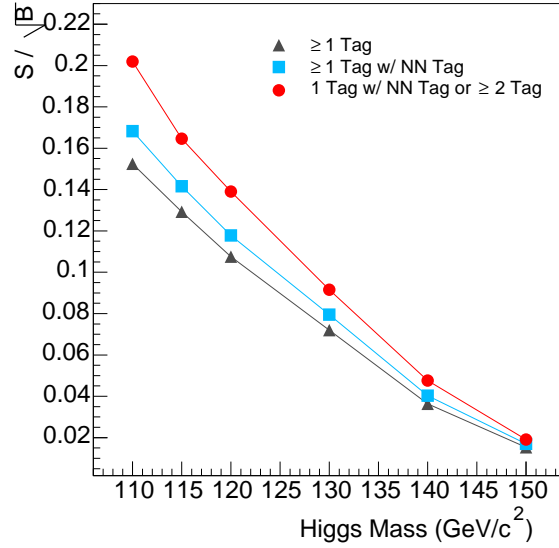


FIG. 6: Comparison of significance obtained from various  $b$ -tagging strategies. “Tag” and “NN Tag” represent SECVTX and NN  $b$ -tagging, respectively. The filled circles correspond to the combined analysis which treats disjoint samples with exactly one NN  $b$ -tag and two SECVTX tags separately.

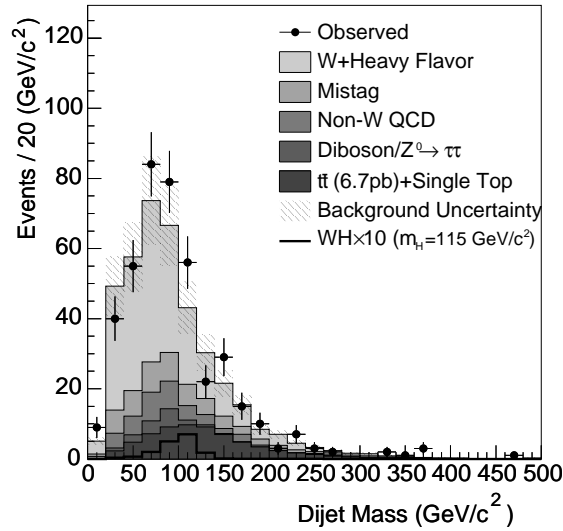


FIG. 7: Dijet mass distribution in  $W+2$  jets events including exactly one SECVTX  $b$ -tagged jet that passes the NN  $b$ -tagging filter. The contributions of the various background sources are shown in histogram, while the hatched box on the background histogram represents the background uncertainty.

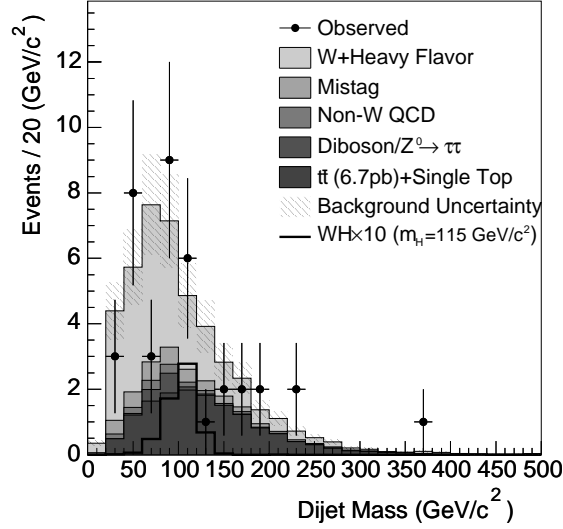


FIG. 8: Dijet mass distribution in  $W+2$  jets events including at least two SECVTX  $b$ -tagged jets.

### A. Binned Likelihood Technique

The number of events in each bin follows the Poisson distribution:

$$P_i(n_i, \mu_i) = \frac{\mu_i^{n_i} e^{-\mu_i}}{n_i!} \quad (i = 1, 2, \dots, N_{\text{bin}}) \quad (11)$$

where  $n_i$ ,  $\mu_i$ , and  $N_{\text{bin}}$  represent the number of observed events in the  $i$ -th bin, the expectation in the  $i$ -th bin, and the total number of bins. The Higgs production hypothesis is constructed by setting  $\mu_i$  to  $\mu_i = s_i + b_i$ , where  $s_i$  and  $b_i$  are the number of signal and expected background events in the  $i$ -th bin. This quantity  $s_i$  can also be written as a product:

$$s_i = \sigma(p\bar{p} \rightarrow W^\pm H) \cdot \mathcal{B}(H \rightarrow b\bar{b}) \cdot \epsilon_{WH} \cdot \int \mathcal{L} dt \cdot f_i^{WH} \quad (12)$$

where  $f_i^{WH}$  is the fraction of the total signal which lies in the  $i$ -th bin. In this case,  $\sigma(p\bar{p} \rightarrow W^\pm H) \cdot \mathcal{B}(H \rightarrow b\bar{b})$  is the variable to be extracted from data. An upper limit on the Higgs boson production cross section times branching ratio  $\sigma(p\bar{p} \rightarrow W^\pm H) \cdot \mathcal{B}(H \rightarrow b\bar{b})$  is extracted by using a Bayesian procedure with a likelihood defined by:

$$L = \prod_{i=1}^{N_{\text{bin}}} P_i(n_i, \mu_i) = \prod_{i=1}^{N_{\text{bin}}} \frac{\mu_i^{n_i} e^{-\mu_i}}{n_i!}. \quad (13)$$

The background prediction  $b_i$  includes contributions from the various background sources described in Sec. V:

$$b_i = N^{TOP} f_i^{TOP} + N^{QCD} f_i^{QCD}, \quad (14)$$

612 where  $f_i^{TOP}$  and  $f_i^{QCD}$  are the fractions of the total number of top (including  $t\bar{t}$  and single  
613 top) and QCD backgrounds (including W+jets, non-W, and diboson) in mass bin  $i$ . There  
614 are systematic uncertainties in the estimates of both the number of signal events and the  
615 expected background. Such uncertainties modify the likelihood to be

$$616 \quad L(\sigma \cdot \mathcal{B}) = \int_{N^{QCD}} \int_{N^{TOP}} \int_{N^{WH}} \prod_{i=1}^{N_{\text{bin}}} \frac{\mu_i^{n_i} e^{-\mu_i}}{n_i!}$$

$$617 \quad \times G(N^{QCD}, \sigma^{QCD}) G(N^{TOP}, \sigma^{TOP}) G(N^{WH}, \sigma^{WH}) dN^{QCD} dN^{TOP} dN^{WH} \quad (15)$$

618 where the  $G(N, \sigma)$  factors are truncated Gaussian densities constraints using the estimated  
619 numbers of events and the associated uncertainties. We assume a uniform prior for  $\sigma \cdot \mathcal{B}$   
620 and integrate the likelihood over all parameters except  $\sigma \cdot \mathcal{B}$ . A 95% credibility level upper  
621 limit on  $\sigma \cdot \mathcal{B}$  is obtained by calculating the 95<sup>th</sup> percentile of the resulting distributions.

622 To measure the expected sensitivity for this analysis, background-only pseudo-  
623 experiments are used to calculate an expected limit in the absence of Higgs boson production.  
624 Pseudo-data are generated by fluctuating the individual background estimates within total  
625 uncertainties. The expected limit is derived from the pseudo-data using Eq. 15.

626 The likelihoods from events with exactly one SECVTX  $b$ -tagged jet passing the NN  $b$ -  
627 tagging filter and events with at least two SECVTX  $b$ -tagged jets criteria are multiplied  
628 together. The systematic uncertainties associated with the pretag acceptance, luminosity  
629 uncertainty, and uncertainty of the  $b$ -tagging efficiency scale factor are considered to be  
630 100% correlated between the two selection channels. Background uncertainties, specifically  
631 on the heavy-flavor fractions and  $b$ -tagging scale factor, are also completely correlated. The  
632 “=1 tag w/ NNtag” selection combined with “ $\geq 2$  Tag” gives the best expected limit, as  
633 expected from the sensitivity study (see Fig. 6).

634 The observed limits as a function of the Higgs boson mass are shown in Fig. 9 and Ta-  
635 ble IX, together with the expected limits determined from pseudo-experiments. An ensemble  
636 of limits from pseudo-experiments and the observed limit for each Higgs boson mass point  
637 are shown in Fig. 10. The limit in the low mass region is at most two standard deviations  
638 higher than the expected limit, but this is consistent with a statistical fluctuation in the  
639 dijet mass distributions (see Fig. 7) around  $m_H = 115 \text{ GeV}/c^2$ . Such a fluctuation is much  
640 larger than the expectation for SM Higgs boson production in this channel.

641 The search sensitivity is improved significantly with respect to previous searches, about  
642 30% beyond the expectations from simple luminosity scaling. The two main effects are the

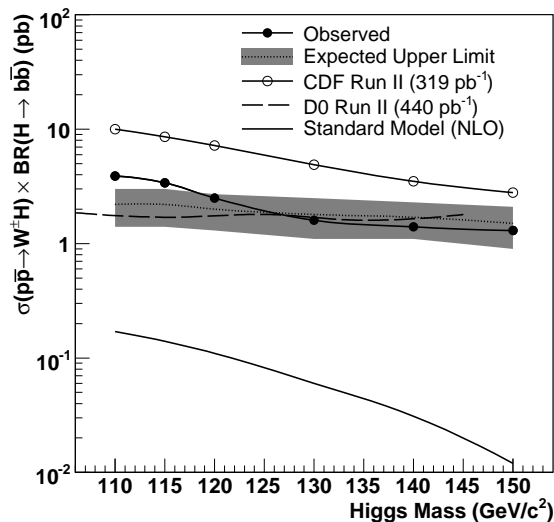


FIG. 9: 95% confidence level upper limit on  $\sigma(p\bar{p} \rightarrow WH) \cdot \mathcal{B}(H \rightarrow b\bar{b})$  with an integrated luminosity of  $1 \text{ fb}^{-1}$  obtained from the combined likelihood between events with exactly one SECVTX  $b$ -tag passing the NN  $b$ -tagging and events with at least two SECVTX  $b$ -tagged jets. The previous CDF data [7] and recent D0 data [8] are shown for comparison.

643 separation of the  $b$ -tagged data sample into single- and double-tagged events, and the NN  
 644 filter applied to the single-tag sample.

## 645 IX. CONCLUSIONS

646 We have presented a search for the standard model Higgs boson in the  $\ell\nu b\bar{b}$  final state  
 647 expected from  $WH$  production. The event selection includes an additional neural network  
 648  $b$ -tag filter to reduce the background contributions from light flavor and charm quark jets.  
 649 This improvement, along with a total dataset corresponding to  $1 \text{ fb}^{-1}$ , allows us to improve  
 650 the upper limit on Higgs boson production. We set a 95% confidence level upper limit on the  
 651 production cross section times branching ratio varying from 3.9 to 1.3 pb for Higgs boson  
 652 masses 110 to 150  $\text{GeV}/c^2$ .

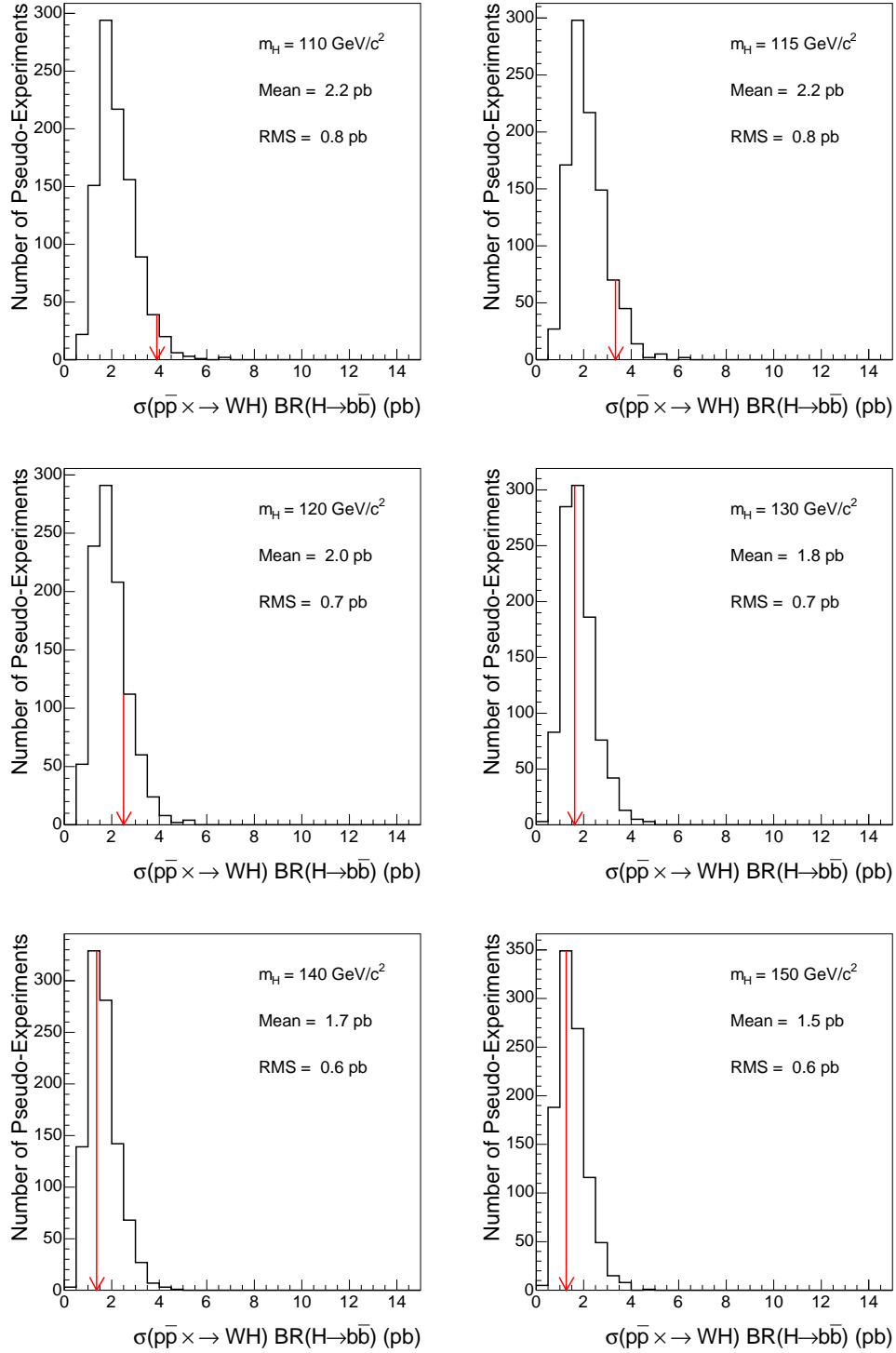


FIG. 10: Results of 95% confidence level limits obtained from the combined likelihood in pseudo-experiments. The arrows indicate the observed limits.



Higgs Mass GeV/c <sup>2</sup>	Upper Limit (pb)		
	Observed	Expected	SM
110	3.9	2.2±0.8	0.16
115	3.4	2.2±0.8	0.13
120	2.5	2.0±0.7	0.10
130	1.6	1.8±0.7	0.060
140	1.4	1.7±0.6	0.030
150	1.3	1.5±0.6	0.011

TABLE IX: Observed and expected upper limits on  $\sigma(p\bar{p} \rightarrow WH) \cdot \mathcal{B}(H \rightarrow b\bar{b})$  at 95 % C.L., compared to the SM production rate calculated at NNLO.

### 653 Acknowledgments

654 We thank the Fermilab staff and the technical staffs of the participating institutions for  
655 their vital contributions. This work was supported by the U.S. Department of Energy and  
656 National Science Foundation; the Italian Istituto Nazionale di Fisica Nucleare; the Ministry  
657 of Education, Culture, Sports, Science and Technology of Japan; the Natural Sciences and  
658 Engineering Research Council of Canada; the National Science Council of the Republic of  
659 China; the Swiss National Science Foundation; the A.P. Sloan Foundation; the Bundesmin-  
660 isterium für Bildung und Forschung, Germany; the Korean Science and Engineering Foun-  
661 dation and the Korean Research Foundation; the Science and Technology Facilities Council  
662 and the Royal Society, UK; the Institut National de Physique Nucleaire et Physique des Par-  
663 ticules/CNRS; the Russian Foundation for Basic Research; the Comisión Interministerial de  
664 Ciencia y Tecnología, Spain; the European Community’s Human Potential Programme; the  
665 Slovak R&D Agency; and the Academy of Finland.

- 
- 666 [1] P. W. Higgs, Phys. Rev. Lett. **13**, 508 (1964).  
667 [2] R. Barate et al. (ALEPH, DELPHI, L3, and OPAL collaborations and the LEP Working  
668 Group for Higgs boson searches), Phys. Lett. **B565**, 61 (2003), hep-ex/0306033.  
669 [3] J. Alcaraz et al. (ALEPH, DELPHI, L3, and OPAL collaborations and the LEP Electroweak

670 Working Group), Tech. Rep. CERN-PH-EP-2006-042 (2006), hep-ex/0612034.

671 [4] T. Han and S. Willenbrock, Phys. Lett. **B273**, 167 (1991).

672 [5] A. Djouadi, J. Kalinowski, and M. Spira, Comput. Phys. Commun. **108**, 56 (1998), hep-  
673 ph/9704448.

674 [6] A. Abulencia et al. (CDF collaboration), Phys. Rev. **D75**, 012010 (2007), hep-ex/0612015.

675 [7] A. Abulencia et al. (CDF collaboration), Phys. Rev. Lett. **97**, 081802 (2006), hep-ex/0605124.

676 [8] V. M. Abazov et al. (D0 collaboration), Phys. Lett. B (to be published), hep-ex/0712.0598.

677 [9] D. Acosta et al. (CDF collaboration), Phys. Rev. **D71**, 052003 (2005), hep-ex/0410041.

678 [10] D. Acosta et al. (CDF collaboration), Phys. Rev. **D71**, 032001 (2005), hep-ex/0412071.

679 [11] L. Balka et al., Nucl. Instrum. Methods **A267**, 272 (1988).

680 [12] S. Bertolucci et al., Nucl. Instrum. Methods **A267**, 301 (1988).

681 [13] M. G. Albrow et al., Nucl. Instrum. Methods **A480**, 524 (2002).

682 [14] F. Abe et al. (CDF collaboration), Phys. Rev. **D45**, 1448 (1992).

683 [15] A. Bhatti et al., Nucl. Instrum. Methods **A566**, 375 (2006), hep-ex/0510047.

684 [16] G. Ascoli et al., Nucl. Instrum. Methods **A268**, 33 (1988).

685 [17] T. Dorigo (CDF collaboration), Nucl. Instrum. Methods **A461**, 560 (2001).

686 [18] E. J. Thomson et al., IEEE Trans. Nucl. Sci. **49**, 1063 (2002).

687 [19] D. Acosta et al. (CDF collaboration), Phys. Rev. Lett. **94**, 091803 (2005), hep-ex/0406078.

688 [20] A. Abulencia et al. (CDF collaboration), Phys. Rev. Lett. **97**, 082004 (2006).

689 [21] C. Peterson, T. Rönigvaldsson, and L. Lönnblad, Comput. Phys. Commun. **81**, 185 (1994).

690 [22] A. Abulencia et al. (CDF collaboration), Phys. Rev. **D74**, 072006 (2006), hep-ex/0607035.

691 [23] A. Abulencia et al. (CDF collaboration), Phys. Rev. Lett. **97**, 082004 (2006), hep-ex/0606017.

692 [24] M. L. Mangano, M. Moretti, F. Piccinini, R. Pittau, and A. D. Polosa, J. High Energy Phys.  
693 **07**, 001 (2003), hep-ph/0206293.

694 [25] G. Corcella et al. (2001), hep-ph/0201201.

695 [26] J. Campbell and R. K. Ellis, Phys. Rev. **D65**, 113007 (2002), hep-ph/0202176.

696 [27] M. Cacciari, S. Frixione, M. L. Mangano, P. Nason, and G. Ridolfi, J. High Energy Phys. **04**,  
697 068 (2004), hep-ph/0303085.

698 [28] B. W. Harris, E. Laenen, L. Phaf, Z. Sullivan, and S. Weinzierl, Phys. Rev. **D66**, 054024  
699 (2002), hep-ph/0207055.

700 [29] T. Sjöstrand et al., Comput. Phys. Commun. **135**, 238 (2001), hep-ph/0010017.

- 701 [30] A. Abulencia et al. (CDF collaboration), Phys. Rev. **D73**, 032003 (2006), hep-ex/0510048.
- 702 [31] J. Pumplin et al., J. High Energy Phys. **07**, 012 (2002), hep-ph/0201195.